CHALMERS
UNIVERSITY OF TECHNOLOGY

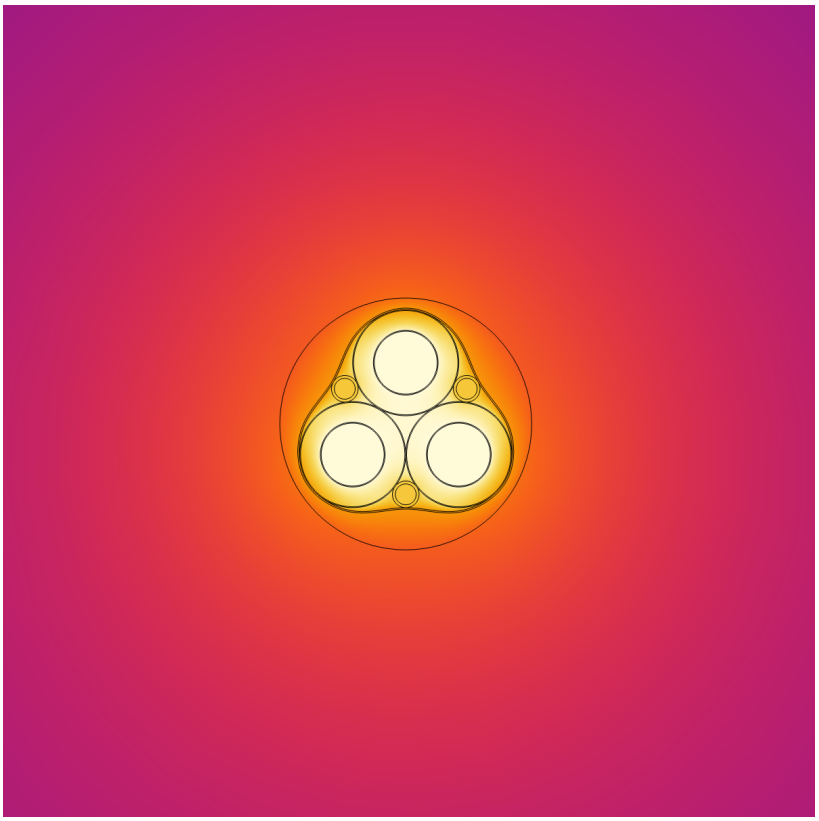

Thermal Aging in Power Cables

How Thermal Stress Affects Aging in Underground 10 kV Cables

Master's thesis in Sustainable Electric Power Engineering and Electromobility

PETTER ENGSTRÖM

DEPARTMENT OF ELECTRICAL ENGINEERING
CHALMERS UNIVERSITY OF TECHNOLOGY
Gothenburg, Sweden 2026
www.chalmers.se

Master's thesis 2026

Thermal Aging in Power Cables

How Thermal Stress Affects Aging in Underground 10 kV Cables

PETTER ENGSTRÖM

CHALMERS
UNIVERSITY OF TECHNOLOGY

Department of Electrical Engineering
Division of Electric Power Engineering
Chalmers University of Technology
Gothenburg, Sweden 2026

Thermal Aging in Power Cables
How Thermal Stress Affects Aging in Underground 10 kV Cables
Petter Engström

Supervisor: Yuriy Serdyuk, Professor, Department of Electrical Engineering
Examiner: Peiyuan Chen, Associate Professor, Department of Electrical Engineering

Master's Thesis 2026
Department of Electrical Engineering
Division of Electric Power Engineering
Chalmers University of Technology
SE-412 96 Gothenburg
Telephone +46 31 772 1000

Cover: The temperature of the AXAL cable and the surrounding area at a specific time.

Typeset in LaTeX
Gothenburg, Sweden 2026

Abstract

The electricity demand in Gothenburg is projected to increase over the next years. The current grid is pushed closer to its operational limits. For underground power cables, thermal stress is the leading cause of degradation, and to maintain a reliable grid, understanding the relationship between aging, current, and environment is crucial.

The aim of this thesis is to design and analyze a model to quantify the thermal aging of the cable's insulation for Gothenburg's 10 kV grid. This work uses two cables, an older model with oil impregnated paper insulation, named FCJJ, and a modern one that uses cross-linked polyethylene insulation, called AXAL. With the simulation program COMSOL Multiphysics, partial differential equations (PDE) were solved for electromagnetic and thermal calculations. This was conducted for one, two, and three cable configurations. In addition, a sensitivity analysis was carried out to assess the effects of vital parameters, including varying loads during the different seasons, two scenarios of soil drying, which lead to lower thermal conductivity, and a scenario of higher load. The simulation data was integrated with the Arrhenius equations to calculate aging.

The results show that while the composition of the one and two cables did not exceed their thermal rating for both cables, the three cables operated with smaller margins. As a result, this implies that mutual heating has an immense affect on the temperature of the cables and the surrounding soil. with this configuration the AXAL cables reached 81.1 ° C, which operates below the XLPE 90 ° C rated temperature. However, scenarios with drying soil and higher current exhibit the system's potential vulnerability. With the worst case scenario where the surrounding soil dried up, the temperature spiked to over 125 ° C, the thermal aging factor reached 47 times the relative aging for which the cables were constructed. As a result, this would be catastrophic for the cable and the entire system, as it could lead to breakdown, warping of the conductors. Nevertheless, this scenario was deemed unrealistic due to the intervention of the grid's monitoring systems and the mitigation of the current. However, it is theoretically possible to happen, which concludes that understanding the phenomenon is essential when designing and monitoring underground cables.

The thesis illustrates that the three FCJJ and AXAL cable configurations can handle loads under normal conditions. However, thermal instability in underground power cables, cable placement, soil moisture, and load are major factors. These insights are vital when planning grid projects and implementing the dynamic cable rating.

Keywords: Rated temperature, thermal conductivity, thermal aging, mutual heating, XLPE, oil impregnated paper insulation, Arrhenius equation, COMSOL Multiphysics, 10 kV, power cable.

Acknowledgements

My profound gratitude and thank goes to Associate Professor Peiyuan Chen for helping me through the up and downs during the project. With the utmost help whenever i had any question or suggestion. Lastly, a special thanks goes to professor Yuriy Serdyuk for assisting and guiding me with the COMSOL simulations.

Petter Engström, Gothenburg, May 2026

List of Acronyms

Below is the list of acronyms that have been used throughout this thesis listed in alphabetical order:

FEM	Finite-element method
PDE	Partial differential equations
AC	Alternating current
DC	Direct current
XLPE	Cross-linked polyethylene
PILC	Paper Insulated lead sheath Cable
PIC	Oil-impregnated paper
PE	Polyethylene
PVC	Polyvinyl chloride

Contents

List of Figures

List of Tables

1
Introduction

1.1 Background

In Göteborg, the demand for electrical networks is expected to increase substantially in the coming years, and securing land for new cable installations will be difficult[1]. It is desirable to improve the efficiency of existing grids in various aspects, but the most important is to lower the cost of the electrical distribution. The 10 kV grid is built as an n-1 loop structure to ensure redundancy. However, increasing power consumption means that cables are operating closer to their limits.

When the current reaches close to the capacity of the cable, it should be monitored to prevent failure. For underground cable operations, thermal stress is the primary factor in insulation material degradation [2]. Although the highest cable loading typically occurs only during a short period of the year, this is often what causes the most thermal stress. With higher load demand, power cables will deteriorate faster and the product lifetime will be reduced. The increased power consumption has led to this happening faster than before. With an industry and society that needs an increasing amount of electricity and the transition that is taking place will only demand more from the grid.

In addition, climate and weather affect the power cables. With colder climates, maximum power consumption drives load peaks during the winter period. That increases the temperature and accelerates the aging faster. In summer, places need large amounts of cooling or an array of solar panels will have energy spikes on the grid, and the charging of electric vehicles will increase it further[3]. Thus, both periods will be investigated during this thesis. A deeper understanding of how temperature affects the soil and the stability of the insulation material will be analyzed.

1.2 Aim

The aim of this project is to evaluate the thermal aging of the cable insulation by modeling typical cables used in the 10 kV grid in Göteborg.

1.3 Scope

For this project a thorough analysis of how the load, cable placement, and environmental aspects affect the aging will be established. The focus will be on two different 3-phase cables, one older oil-impregnated paper insulated cable, and secondly, a modern XLPE cable. These cables have different materials, properties, and geometries, which need to be sourced and analyzed. The cables will have the same configurations and scenarios to see the affects of every parameter. The first setup is with only one cable in the ground, then two cables, and in the end three cables. All models are provided with a normal condition simulation, a dry soil scenario and additionally with a completely dry soil scenario. The three cables design will be explored further, thus, a higher current scenario is added.

For the simulation program, COMSOL is used which will simulate a time dependent temperature in the cables and ground. The first step in COMSOL is designing a geometry, and then every geometry is applied a material with properties. Lastly, the model defines the physical behavior. Once the first model is completed, the simulation will move on to two cables and later three cables. This is done for both the AXAL and FCJJ cables. In the end, the FCJJ cable will have three 3-phase cables in the ground with four different scenarios simulated. In addition, there are two scenarios for both the one- and two cable setups. Similarly, The same goes for the AXAL cable with the addition of one more cable simulation due to evaluating skin effect.
Furthermore, we implement the result in Arrhenius equations for the aging calculations and, lastly, evaluate the data with a sensitivity analysis for a thorough breakdown of what impacts the thermal aging.

1.4 limitations

The thesis focuses on Gothenburg's electrical grid and with that the Swedish regulations for the grid. The 10 kV is the voltage that will be investigated. Not all material parameters and properties will be known for the design. Thus, assumptions will be made. Climate scenarios and environmental temperatures are estimated using data from SMHI. Furthermore, the thesis assumes a symmetric environment for the 2D design, which may not capture the depth variations that 3D may present. Lastly, localized hotspots and defects will not be investigated, nor will breakdowns or discharges.

2
Theory

A literature study was conducted to describe the theoretical concepts necessary to explain the modeling of a power cable. The concepts explain the fundamental effect of thermal stress on material degradation.

2.1 Electromagnetic theories

2.1.1 Gauss's law

Gauss's law for magnetism states that the divergence of the magnetic flux density **B** is zero,

$$\nabla \cdot \mathbf{B} = 0. \tag{2.1}$$

This implies that there are no isolated magnetic charges. As a result, the magnetic field lines do not have a inception or a conclusion, only continuous closed loops. When a new magnetic flux passes through a closed volume, it must also exit it, thus maintaining a net flux of zero [4].

To solve this mathematically, the magnetic vector potential **A** is introduced. With the relationship between **A** and **B**, the calculation of the magnetic field will be simpler. The magnetic flux density equation can be expressed as

$$\mathbf{B} = \nabla \times \mathbf{A} \tag{2.2}$$

2.1.2 Faraday's law

Faraday's law states that a time varying magnetic field induces a circulation electric field and is expressed with

$$\nabla \times \mathbf{E} = -\frac{\partial \mathbf{B}}{\partial t}. \tag{2.3}$$

The negative rate of change of the magnetic flux density **B** is proportional to the curl of the electric field **E**. This generates an electromotive force and as a result creates eddy currents in conductive materials[4]. Where V is the scalar electric potential and a simplified expression for the electric field is,

$$\mathbf{E} = -\nabla V - \frac{\partial \mathbf{A}}{\partial t}. \tag{2.4}$$

2.1.3 Ampère's law

This equation describes the relationship between the applied current and the resulting magnetic flux. As it relates to the curl of the magnetic field intensity **H** and the total current density **J**, expressed as:

$$\nabla \times \mathbf{H} = \mathbf{J}. \tag{2.5}$$

J is sum of all the currents, including external, conduction and displacement currents. Thus, the magnetic field is generated by a time dependent electric field or by any moving charge[4].

2.2 Fourier's law

The transport of thermal energy through a solid is a phenomenon described by Fourier's law. This relationship describes the rate of heat transfer as an function of heat distribution in a medium. The law states that the heat flux is directly proportional to the temperature gradient, functioning as a link between the energy transport procedure and the systems thermal state[5]. Fourier's law expressed as:

$$q = -k\nabla T \tag{2.6}$$

where k is the thermal conductivity of the materials, ∇T is the gradient temperature vector, and q is the local heat flux.

2.3 Thermal aging

Thermal stress is the main cause of aging for power cables and other electrical components in high voltage operations. As the temperature increases, the degradation of the insulation material accelerates, leading to an increased aging rate. This indicates that elevated ambient temperature or restricted heat dissipation, caused by high thermal resistivity of the soil, increases the probability of cable failure for underground cables[2]. Today failure caused by thermal stress is infrequent, future system aims to operate closer to thermal limits. As a result, a complete understanding of the aging phenomenon is crucial.
In the context of power cables, thermal stress affects the insulation material and its longevity. The Arrhenius equation is a formula that describes the correlation between thermal stress and insulation material degradation [6]. Thus, it is a chemical process driven by thermal energy, and higher temperature trigger numerous chemical reactions inside the material[7]. The Arrhenius equation can be written as:

$$k_d = A \cdot e^{-B/T} \tag{2.7}$$

where k_d is the degradation rate, A is the constant that determines the probability of molecular coalitions during the chemical reaction. T is the temperature and B is the aging rate constant defined by $B = E_a/k_B$. E_a is the activation energy that causes

the aging of the material and k_B is the Boltzmann constant. A new connection for the lifetime L can be written as

$$L = L_0 e^{-B/T} \tag{2.8}$$

The temperature dependence in the exponent is expressed [7] as the thermal stress, cT. This gives,

$$cT = \left(\frac{1}{T_{ref}} - \frac{1}{T}\right)$$

T_{ref} is the temperature of the material rated and the lifetime equation can be expressed as:

$$L = L_0 e^{-BcT} \tag{2.9}$$

To make it easier for cable analysis, the aging rate of the cable's rated temperature T_{ref} is used as a base to evaluate aging rate of a cable at a given temperature T

$$v = \frac{k(T)}{k(T_{ref})}.$$

This ratio can be defined as the relative aging factor v. Substitute (2.7) into the above equation:

$$v = \exp\left(\frac{E_a}{k_B} \cdot \left(\frac{1}{T_{ref}} - \frac{1}{T}\right)\right) \tag{2.10}$$

The lost lifetime can be calculated according to [8]

$$L_{loss} = \int_{t_1}^{t_2} v(T)\, dt \tag{2.11}$$

With the connections, it can be established that the cable's lifetime is heavily dependent on the operational temperature. As a result, the lifetime can be longer than designed for, provided that the cable is operating below the rated temperature.

2.4 Properties of soil

The ground temperature influences the thermal conductivity of the cable's surroundings. The soil has a large volumetric heat capacity, which has a large thermal inertia. Thus, temperature fluctuations occur at a slow rate[9]. For Sweden near the Gothenburg area, the ground temperature fluctuates between 0 ° C and 15 ° C throughout the year[10]. Data for ground temperature in Sweden are collected in a few selected places. Thus, using the air temperature to estimate the temperature of the ground is a possible approach.

2.4.1 Thermal resistivity

Thermal resistivity is the ability of the material to withstand the flow of heat[11]. Thus, it governs the rate at which the heat can be dissipated during load or installation. Thermal resistivity and thermal conductivity will be mentioned numerous times interchangeably during the thesis and the relationship is inverse of one another.

$$r_\lambda = \frac{1}{k}, \tag{2.12}$$

With r_λ being the thermal resistivity, k the thermal conductivity. Sweden uses a value of 1 $\mathrm{K \cdot m/W}$ under normal conditions and $2,5$ $\mathrm{K \cdot m/W}$ in uncertain situations for the thermal resistivity of the soil[12] [10].
The thermal resistivity is not constant and depends on local conditions; for instance, dry soil has higher resistivity than wet soil. As a result, a selected soil changes the resistivity depending on if moisture changes occur [11]. Thus, an increase in cable temperature or alternatively a change in the condition that contributes to a higher temperature in the surrounding soil can lead to soil drying out. Consequently, the heat dissipation will decrease further, and it might cause the temperature to rise additionally. This state is called thermal instability and phenomenon that causes a rapid rise in temperature in the cable. Thus, having a surrounding soil with rapid moisture recovery capacity to the desired condition is crucial[11]. For a conventional power grid with high loads in the morning and evening and lower consumption during the night, the risk of thermal instability is low. However, a constant high load over long periods of time will increase the risk of thermal instability.

2.4.2 Cable placement

Underground cables are generally placed directly on the ground at a depth of 0.6 to 1 meters. Alternatively, for optimal conditions, soil with strong thermal properties is placed surrounding the cable. Additionally, in cities where space is a problem, cables can be placed in ducts, pipes, or, on ladders, and using existing space underground[13][9]. The placement of cables together increases the overall temperature. In addition, placement influences temperature. As a result, two cables with no space in between will generate more heat compared to two cables placed 10cm apart. Thus, an ideal placement for optimal heat distribution and cost-effective results is desired.

3
Cable design and characteristics

3.1 Construction

The power cables structure consists of mainly two parts, a conductor and insulation. However, for underground cables, some additional protection is needed, such as a semi-conducting screen, a metallic sheath, and an anti-corrosion sheath.

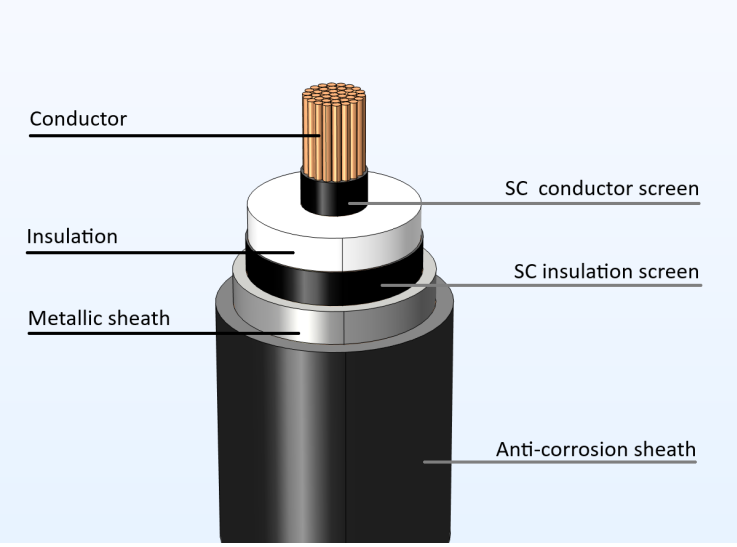

Figure 3.1: Schematic illustration of the cable construction, showing the conductor, insulation, semiconducting screens, and metallic sheath layers.

3.1.1 Conductor

The metal core that carries the electrical current, predominantly constructed of aluminum or copper. The latter exhibits lower electrical resistivity, although aluminum costs significantly less, approximately 50%. However, to transmit the same load current as the copper cable, the cross-sectional area of an aluminum cable will be larger. As a result, insulation material expenses increase relative to copper cable[13]. The conductor designs consist of different geometric profiles including circular, oval, or sector shaped [14].

3.1.2 Inner and outer SC screen

A layer of semiconducting material that facilitates a gradual transition of the electric field for the different layers of elements. Thereby, reducing localized stress and preventing dielectric breakdown. Thus, modern power cables are provided with one inner screen between the conductor and the insulation and one outer between the insulation and the metallic sheath. Alternatively, named conductor screen and insulation screen.[13].

3.1.3 Insulation

The insulation material can be a liquid, a gas, or a solid. The fundamental purpose of the insulation is to ensure the galvanic isolation trough, preventing the current to leak out of the conductor to the other material of the cable, other components, other cables, or the environment. When a current flows through the conductor, there is a potential difference across the dielectric that creates an electric field between inner and outer boundaries of the insulation. As a result, the insulation material requires enough strength to withstand electric stress and voltage transients[13]. Common insulation material in Sweden are cross-linked polyethylene(XLPE) and oil-impregnated paper(PIC) for older cables still in operation.

3.1.4 Metallic sheath

A solid metal sheath or wires placed over the insulation or the insulation screen. Its primary function is to prevent electrical field leakage. The sheath functions as a conductor for various types of currents, eddy currents, fault current, charging currents and surge currents[15]. With paper insulated cables, lead is frequently utilized as the sheath due to its water resistant capabilities[13].

3.1.5 Armour

An extra metallic layer for enhanced mechanical robustness and strength. Usually critical for submarine cables or underwater installations. The layer is made up of steel wires of steel tapes[13].

3.1.6 Outer sheath

Often called a sheath, jacket, or anti-corrosion sheath. The outer layer of the cable with a tough, waterproof and UV-resistant plastic layer to protect the cable from the environment. The material is PVC or PE[13].

3.2 Power loss

This section analyzes power loss and its effects on temperature. There are a number of factors that affect the temperature of a cable. Mainly, these include heat generation for the different cables elements and including the ability of the surrounding environment to dissipate heat. Heat generation occurs in the conductor, insulation, armor, and the metallic sheath. The heat dissipation capacity is largely determined by the choice of material, placement of the cables, installation, and the soil's thermal conductivity.

3.2.1 Losses

In general, there are two categories of power losses, resistive losses that occur due to the current conductor material and losses due to the voltage difference on the insulation, the dielectric loss[13][16].

3.2.2 Resistive losses

Resistive losses are a function of the cable's load current I. P are the losses for the conductor and can be calculated as

$$P_c = RI^2, \tag{3.1}$$

where R is the AC resistance for the conductor, which in turn, the AC resistance depends on the temperature, the conductors DC resistance, skin, and proximity effects. The skin effect is discussed later in this thesis, in section 3.4. The proximity effect is caused by the alternating magnetic field of neighboring current carrying conductors. As a result, from an increase in skin effect and proximity effect, a higher effective resistance will develop, hence, increasing the losses in the cable[17].

Resistive losses may occur in the metallic sheath and the armor. These currents are categorized as eddy currents and circulating currents. Thus, Eddy current arises when the cable is subjected to alternating magnetic fields. Circulating currents are caused by induced currents circulating between the sheaths or between the sheaths and the ground. Similarly as the sheaths, currents are induced in the armor, circulating through its grounding system. As a result, resistive losses are generated in the armor. Underground cables are frequently grounded at a minimum in one place and have a considerable effect on losses[13].

3.2.3 Dielectric losses

Since the insulation functions as a capacitor between the conductor and the screen, currents and an electric field are formed throughout the insulation. The electric field alternates with the frequency of the system, causing the insulation dipoles to oscillate. Thus, heat is generated. These are known as dielectric losses P_d, and depends on the voltage of the cable and the insulation material properties[13]. The calculation are:

$$P_d = 2\pi f C V_0^2 tan\delta, \tag{3.2}$$

with f as the frequency, C the capacitance over the insulation, V_0 the phase current, and $tan\delta$ being the dielectric loss factor[13].

However, Dielectric losses are largely negligible for XLPE and paper insulated cables at voltages up to 60 kV. The dielectric losses are roughly 0.1% of the resistive losses for XLPE cables. Generally, dielectric losses can be neglected for cables within a distribution network[17][13].

3.3 Temperature limit for cables

The current carrying capacity of a cable, or ampacity, is primarily limited by what the insulation can tolerate[18]. The impacts of higher temperatures could lead to a decrease in insulation properties for paper insulated cables(PIC), in addition to deformation and aging for PIC, XLPE, PE and PVC[17]. Thus, in overtime, higher temperatures could lead to insulation failure. In power cables, thermal or electrical stress-induced insulation failure often leads to electrical failure [7].
The thermal rating of the cables is determined by the temperature that the insulation material can tolerate. The area most at risk is closest to the conductor. Paper, XLPE, PVC, PE and EPC are different insulation materials. Paper and XLPE are two common materials for 10 kV cables, with paper and XLPE being typical older and newer models, respectively. XLPE has a rated temperature of 90 ° C [19] and handles most environments well. XLPE is more resistant to deformation than the other materials. PVC is the most moisture resistant; thus, it is used as the sheath material. The thermal rating for papper insulation material is often varied, a common value is 65 ° C [9]. If operating a temperature rated continuously, 90 ° C for XLPE and 65 ° C for PIC, the expected lifetime is up to 40 years and with the ability to reach well above that with a lower nominal load condition[20] [21] [22].

3.4 Skin effect

The skin effect is an electromagnetic phenomenon where a large part of the AC flows in the outer part of a conductor. Therefore, the current density is lower at the center of the conductor. This leads to a relative increase in AC resistance compared to the ohmic DC resistance that directly causes power loss. The skin effect reduces the ampacity of cables, increases active power losses, and contributes to increased thermal stress[17].

The frequency and cross-sectional area of the conductor are factors that increase the skin effect. Copper conductors will start to have an increased skin effect at an area size of 150mm^2 and will increase further with increasing area. Aluminum is similar, except that the skin effect starts to influence 240mm^2 due to higher resistivity.
Solutions to reduce the effect for larger high-voltage cables are the uses of stranded cable design by sectioning the conductor into smaller wires bundled together. For

modeling, the effect of the skin affects performance through two mechanisms. The electromagnetic field distribution and the increased thermal losses.

3.5 Calculating temperature

Generally, there are two methods to study the temperature inside the power cables, the π-model or solving it with differential equations. The latter is examined in Chapter 4. In the π-model heat flow, temperature, thermal resistivity, currents, voltages, and capacitates are represented. Consequently, a circuit can be drawn with the different parameters, such as resistance and capacitance, and, lastly, with circuit theory applied to calculate the temperature. The standard of IEC60853-2 [23], describes the models and parameters used to study the current effect of the cable on heat generation. The π-model is well suited for simpler thermal calculations. However, it is not considered ideal for more complex calculations, such as multi cable installations.

3.6 Cable monitoring

Modern power cables systems use complex designs to monitor the current and temperature to be within the ampacity and thermal limit. As shown in [24], the UK's national grid has implemented a dynamic rating for high voltage cables. The cable specification has a lifetime of 40 years at full load and at thermal rating. At the beginning of the project, overload was regarded an additional benefit, and cables were allowed to reach above the ampacity at a duration of 30 minutes. With the introduction of the monitoring system, the actual ampacity could be predicted 6 hours in advance.

In [25], NKT cable manufacturer developed a cable monitoring system, Valcap. The DTS fibers are placed on or inside the cable. The optical fibers are connected to a DTS unit that collects the measured temperature. All the data collected can be measured in real time. Valcap presents a opportunity to continuously analyze the cables condition for increased flexibility of the cables ampacity.

Systems such as dynamic line rating (DLR), dynamic cable rating (DCR), and DTS are integrated with SCADA for temperature monitoring and flexible ampacity. Two monitoring systems have been mentioned; however, there are numerous alternative systems in operation which differ in complexity and cost.

3.7 Weather and climate dependent load

The power cable load is not a static parameter but a changing variable which depends on the demand on the grid, environmental factors, and weather. Weather is the largest predictor of short term load fluctuations. The winter period has constant high load demand due to the colder climate over longer periods. During summer heatwaves, cooling loads increase demand and increase the peak, which coincides with the highest soil temperature and the lowest heat dissipation[26]. In addition, weather can have a positive effect on ampacity in certain situations. Rainfall can restore soil moisture, resulting in increased thermal conductivity, allowing higher ampacity[27].

Temperature fluctuations can cause mechanical stress on the cable components. During high temperature in the cable that occurs during extreme weather periods. The conductor expands against the insulation material, producing significant pressure, which can cause permanent damage and can cause breakdown[26].

4

Temperature simulations

In order to study the aging of the cables, an accurate model will be designed to calculate the temperature with a simulation program COMSOL Multiphysics. This chapter will present the different simulation methods and how they are implemented with Arrhenius equations.

4.1 Simulation program

COMSOL is a finite-element method (FEM) program that solves coupled partial differential equations (PDEs). COMSOL is used to simulate the magnetic fields of the cable and the thermal stress over time. This section aims to describe the methods used for the simulations and the assumptions made for the cable setup.

4.2 COMSOL workflow

This section explains the importance of a clear work structure in COMSOL:

- **Geometry:** Design the structure with the curated measurements that are represented as computational domains.
- **Materials:** Apply the material properties, such as electrical and thermal conductivity and heat capacity.
- **Physics interfaces and couplings:** How the simulation behaves, which type of simulation one should apply. For this simulation, electromagnetic heating that couples the magnetic fields and heat transfer in solids will be analyzed.
- **Mesh:** Geometry that measures how precise the simulation can be.
- **Study and finishing touches:** Solving in which domain, time or frequency domain.
- **Results:** Review the values and analyze if corrections are needed.

4.3 Setup of model

Two different types of 3-phase cables will be designed, a modern XLPE insulated with an aluminium conductor, NKT AXAL-TT 3X240/50AL 12kV[28], (AXAL) and an older model of a Paper Insulated lead sheath Cable(PILC) with copper conductor, NKT FCJJ 3X95/25,(FCJJ). Both cables are used in the 10 kV local grid of Gothenburg. With current data collected from the cables, a simulation of the cables

will be conducted.

Figure 4.1 illustrates the work flow of design process. Firstly, design a model with a single cable for both the AXAL and the FCJJ cables. The single cable model will simulate a scenario of normal conditions and a different scenario when the soil is drying, which decreases thermal conductivity of the surrounding soil. In addition, a scenario when the soil i completely dried, decreasing the thermal conductivity to the worst case scenario. Before moving further, the AXAL cable needs to be analysed if skin effect is a risk due to the size of the conductor. Thus, the AXAL cable will be evaluated to determine if its possible to simulate a full induction heating model with stranded design, or alternatively if a simplified heat source model can be used. Similarly, the two cable setup is similar to the single cable, only with the addition of a second similar 3-phase cable and a bigger dugout for the soil pavement. The two cables setup will also have the two scenarios of the soil drying. For the three cables setup the same methodology follows with the addition of a third 3-phase cable. However, the three cables will add a scenario with a higher peak current. with the addition of a multiple cables and the simulation takes longer time to perform.

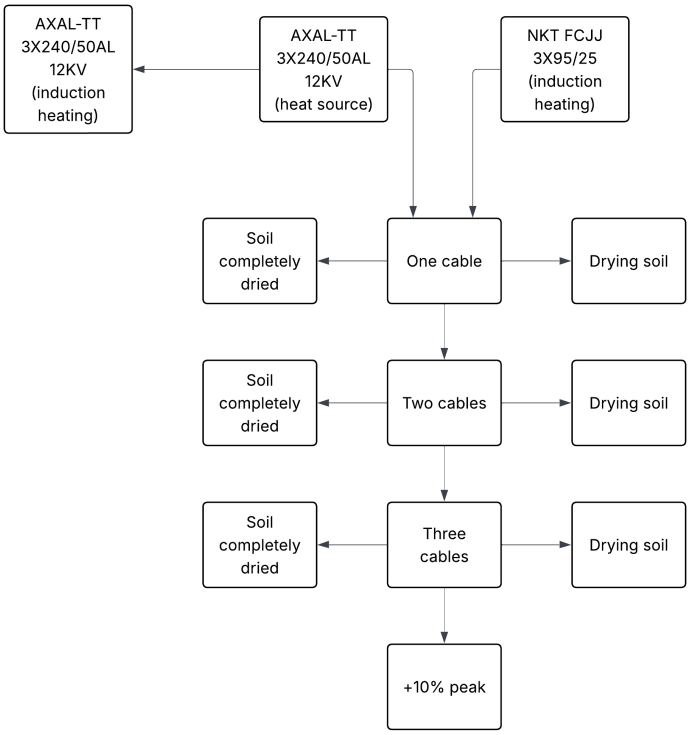

Figure 4.1: The different design versions of the two cables

4.4 Geometry definition

This section explains the cables geometry. A 2D cross-section design with a depth set to 1 meter, giving it a symmetric 2.5D/3D block as the design. Each geometric shape is a different material and the design consists of:

- **FCJJ model:** Pavement soil, initial backfill soil, final backfill soil, PVC sheath, steel lining, waterproofing bitmuen bedding material, lead lining, paper insulation and copper phases. With the conductor being $95mm^2$ for each piece.
- **AXAL model:** Pavement soil, initial backfill soil, final backfill soil, PE sheath, insulation screen, air, XLPE insulation, swelling yarn filler and aluminium for the foil, wires and phases. With the conductor being $240mm^2$ for each piece.

Based on the schematics from [29], a standard for cable placement in Gothenburg, the simplified visualization is shown in figure 4.2. The cable is placed 0.55 meter down into the third layer of soil beneath, the first two layers. The cables are placed 0.05 meters apart. This standard will be used for all the designs.

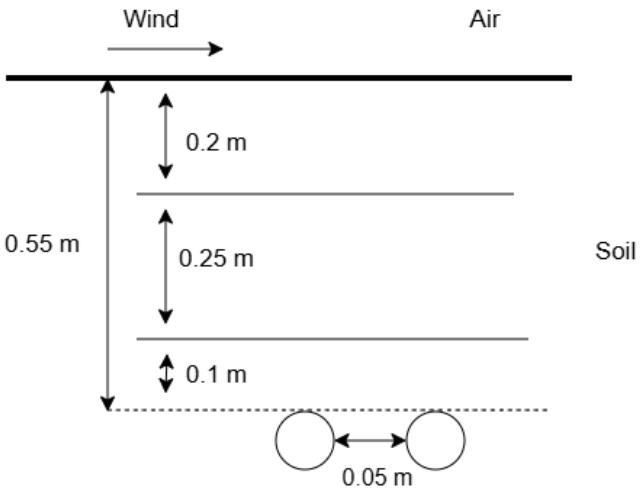

Figure 4.2: Simplified cables placement sketch.

Thus, a design will be implemented with the values shown in figure 4.2. This sketch shows the layout, with air as the top domain and the different soil layers surrounding the cable with each layer having different properties. The two backfill layers are new soil placed before or during cable installation for optimal thermal dissipation and moisture conditions. The outer layer of the soil is the ground already there. This layout of the soil will be used for all designs, the difference will be the final backfill thermal conductivity for the different drying scenarios. Figure 4.3 shows a zoomed out picture of the COMSOL design using the AXAL cable and the 3 surrounding soil layers.

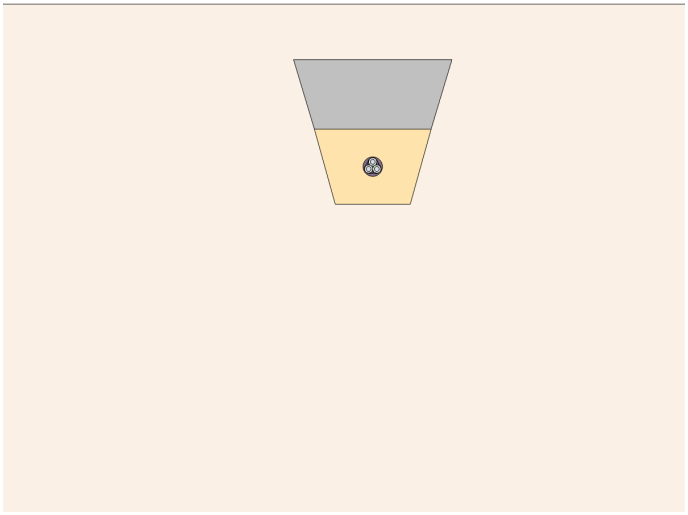

Figure 4.3: A screenshot of the design in COMSOL. The air defined as domain with the black line, pavement soil (beige), initial backfill soil (grey), final backfill soil (yellow) and the AXAL cable.

With the addition of more cables, the design maintain a similar layout, as shown with figures 4.4 and 4.5.

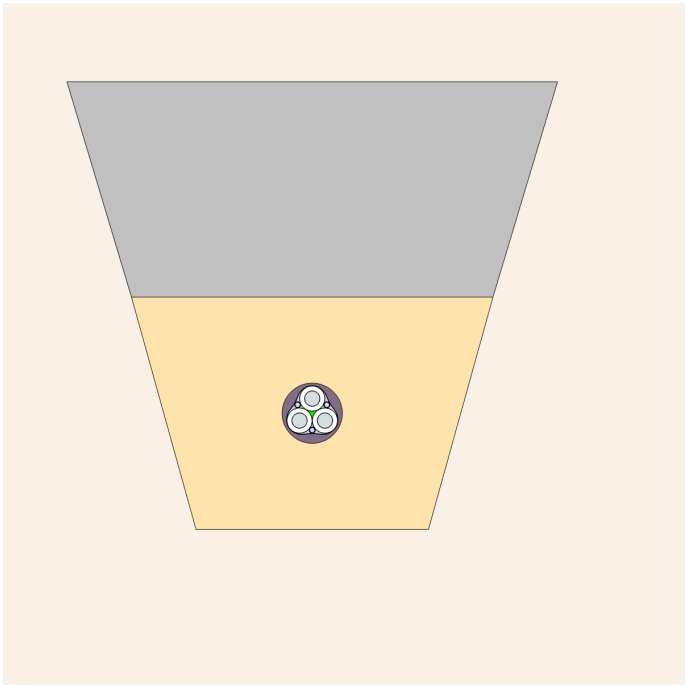

Figure 4.4: COMSOL layout of the AXAL cable design, 3-phase aluminium conductor with XLPE insulation.

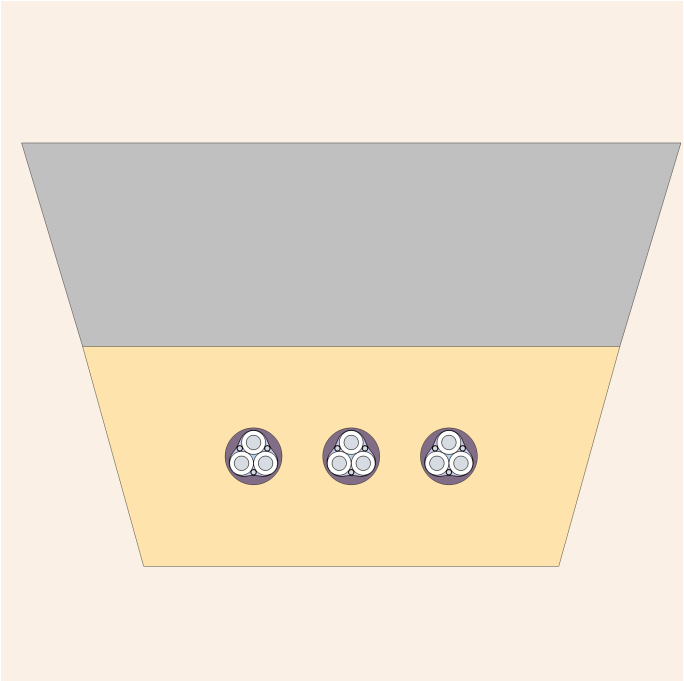

Figure 4.5: Three AXAL cables.

Figures 4.6 and 4.7 shows a zoomed in picture of the different AXAL designs. They are identical except for the conductor phases. The stranded wire design illustrates a cable that has a closer representation to the real life cable. However, the model becomes computationally heavier.

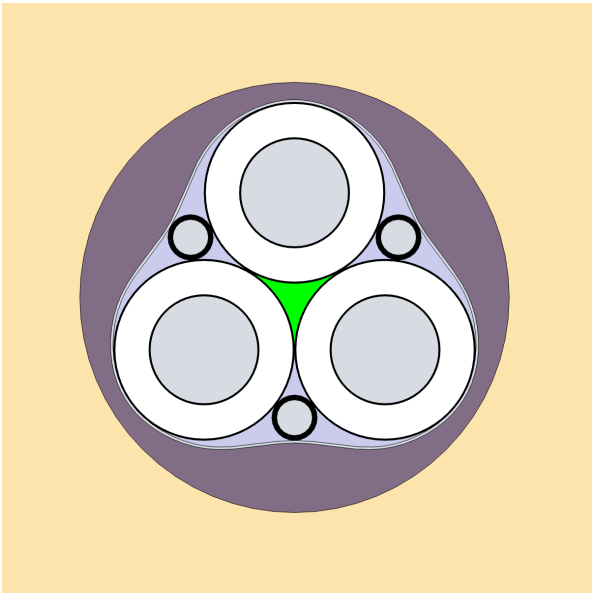

Figure 4.6: Cross section of the AXAL cable. Including three phases, three aluminium wires, aluminium foil (grey), XLPE (white), swelling tape (green),air (light blue), semi- conductor screens (black) and the sheath (dark grey).

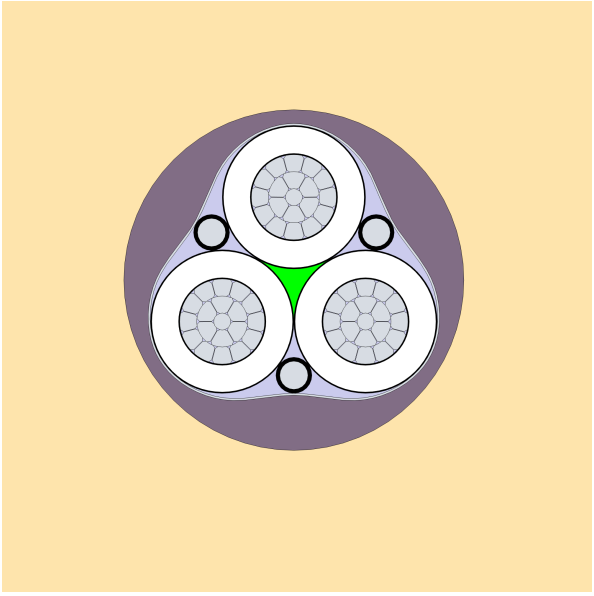

Figure 4.7: Cross section of the AXAL cable, with stranded conductor design. Including three phases, three aluminium wires, aluminium foil (grey), XLPE (white), swelling tape (green),air (light blue), semi- conductor screens (black) and the sheath (dark grey).

FCJJ is a smaller cable compared to the AXAL, the figure 4.8 is more zoomed in. The cable has triangle shaped conductors.

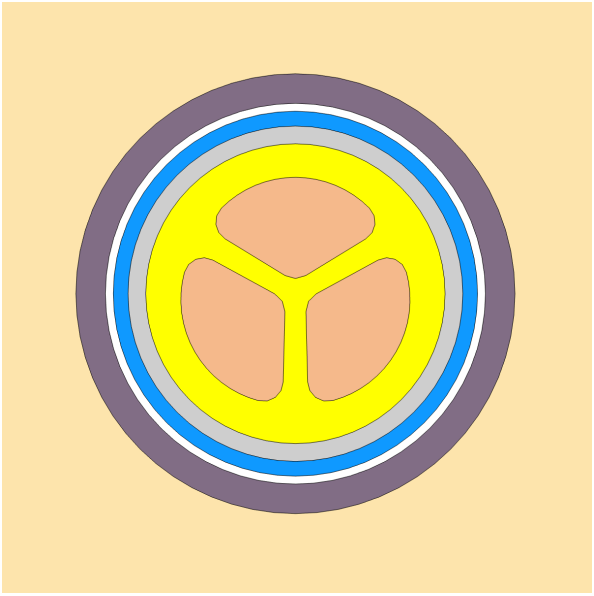

Figure 4.8: Cross section of the paper-insulated lead-covered copper cable. Including three copper phases (brown), paper insulation (yellow), lead lining (grey), bedding (blue), steel lining (white) and the sheath (dark grey).

4.5 Material properties

This section gives an explanation of the material properties and parameters that are implemented. Since the AXAL and FCJJ cables are real cables and company owned, the real data for the material properties are not publicly available and assumptions have been made for the following paramers:
σ = Electric conductivity, C_p = Heat capacity, ρ = Density, k = Thermal conductivity, ϵ_r = Relative permittivity, μ_r = Relative permeability.

4.5.1 Soil

Soil thermal conductivity has a major impact on the thermal stress of the cable. The soil properties were derived from IEC 60287-3-1[30]. The standard model under normal conditions has a surrounding soil with the thermal conductivity of 1 $\mathrm{W/(m \cdot K)}$. The thesis will assess two more adverse conditions. One scenario in which the surrounding soil is drying out with $k = 0.7$ $\mathrm{W/(m \cdot K)}$, and another one with completely dried soil without moisture, to measure operational stress that has the possibility of occurring. The thermal conductivity will be $k = 0.4$ $\mathrm{W/(m \cdot K)}$ in this scenario. The pavement soil and the initial backfill soil properties will be used for all scenarios and simulations. The final backfill soil is used during normal conditions and higher current simulations. Lastly, drying out soil and complete dried soil properties are used instead for the final backfill soil at each respective scenario.

Table 4.1: Values of for the material contents for the three layers of soil and the drying scenarios, used for both cable designs.

Variable	σ	C_p	ρ	k	ϵ_r	μ_r
Unit	[S/m]	$[\mathrm{J/(kg \cdot K)}]$	$[\mathrm{kg/m^3}]$	$[\mathrm{W/(m \cdot K)}]$	[−]	[−]
Pavement soil	0.05	1200	1800	1	5	1
Initial backfill soil	0.01	1000	1900	0.8	5	1
Final backfill soil	0.001	1200	1700	1	3	1
Drying out soil	0.001	1200	1700	0.7	3	1
Complete dried soil	0.001	1200	1700	0.4	3	1

4.5.2 AXAL

Table 4.2: Values of for the material contents for the AXAL cable.

Variable	σ	C_p	ρ	k	ϵ_r	μ_r
Unit	[S/m]	$[\mathrm{J/(kg \cdot K)}]$	$[\mathrm{kg/m^3}]$	$[\mathrm{W/(m \cdot K)}]$	[−]	[−]
Aluminium	3.774×10^7	900	2700	238	1	1
XLPE	1×10^{-15}	2300	930	0.28	2.3	1
PE	1×10^{-15}	1900	930	0.286	2.25	1
Insulation screen	10	2000	1150	0.35	2.25	1
Swelling yarn filler	1×10^{-15}	1700	300	0.05	2	1

4.5.3 FCJJ

Table 4.3: Values of for the material contents for the FCJJ cable.

Variable	σ	C_p	ρ	k	ϵ_r	μ_r
Unit	[S/m]	[J/(kg · K)]	[kg/m^3]	[W/(m · K)]	[−]	[−]
Copper	5.99×10^7	385	8940	400	1	1
Lead	4.55×10^6	127	11340	35.3	1	1
Paper insulation	1×10^{-12}	1500	1100	0.2	3.8	1
Bitmuen	3.2×10^{-9}	1900	1000	0.18	3	1
Steel	4×10^6	475	7850	44.5	1	1
PVC	1×10^{-15}	900	1400	0.17	5	1

4.5.4 Linearized Resistivity

For metals, the temperature changes the resistive properties. To account for this change, linearized resistivity is applied for the metal materials in the magnetic fields physics. The model approximates the change in resistivity ρ as a function of the temperature T.

$$\rho(T) = \rho_{e0}\Big[1 + \alpha\,(T - T_0)\Big] \tag{4.1}$$

ρ_{e0} is the reference resistivity at reference temperature T_0 and α is the resistivity temperature coefficient[31]. With inclusion of linearized resistivity, as a result, the losses and temperatures are again analyzed.

4.6 Value of the current and the weather

Figures 4.9 and 4.10 show data from real life cables with RMS current. The cable values will be used for the simulation. The data is hourly, and every measurement will be considered by the simulation. However, for models with multiple cables, there are different currents flowing in each cable. All the variations will be calculated, nonetheless, for the interest of this work, only the highest currents will be the focus of the calculations.

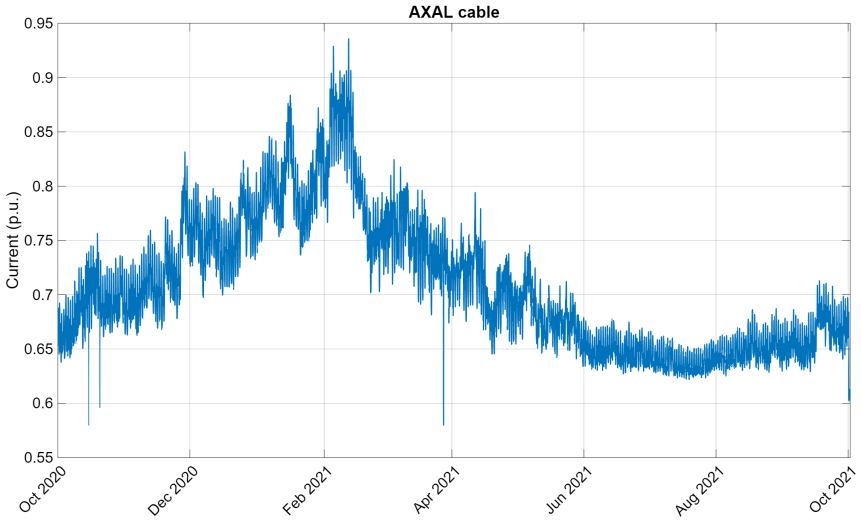

Figure 4.9: The RMS current through the AXAL cable during a year, with the peak in the winter period.

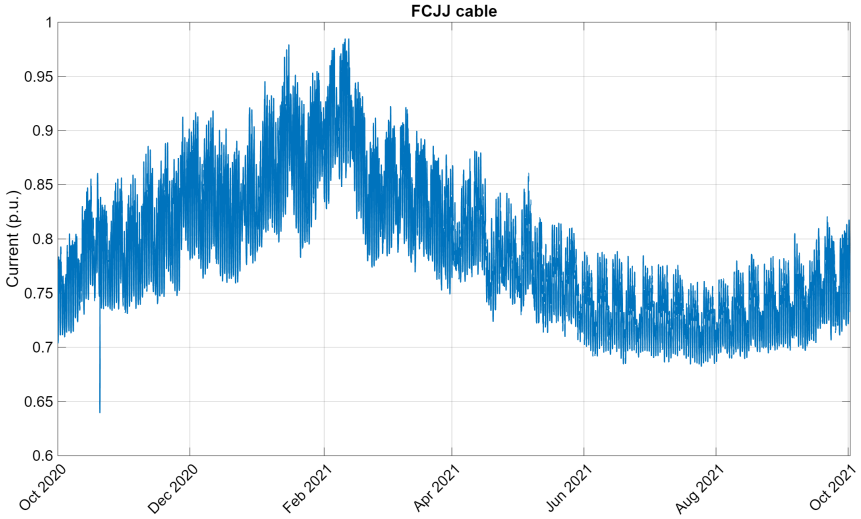

Figure 4.10: The RMS current through the FCJJ cable during a year, with the peak in winter period.

Figure 4.11 shows the temperature data from Gothenburg from SMHI[32] over the same period as the current. The yearly variation exhibits a cyclical behavior and represents the air temperature as an approximated sinus curve. Therefore, the average value of every month will be used. The temperature of the soil follows closely the same pattern. Nevertheless, due to the thermal inertia of the soil, it will be lagging. As a result, the temperature will be lower than that of the air.

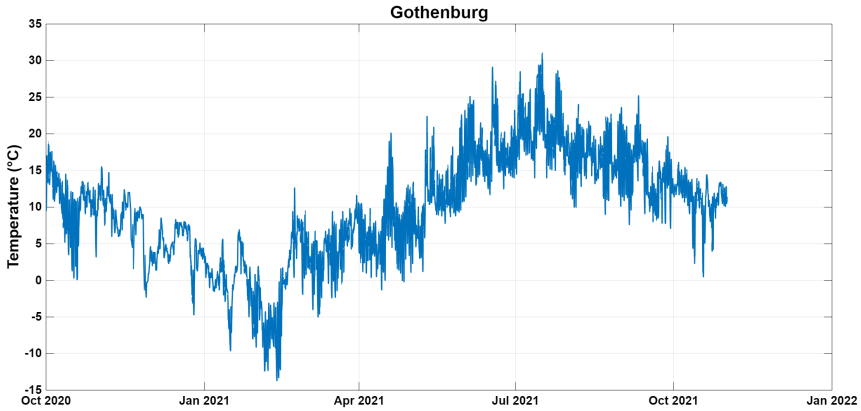

Figure 4.11: The temperature in Gothenburg during the same period as the current measurements. Data from SMHI[32].

4.7 Stranded coils due to Skin effect

The AXAL cable's conductor size of $240mm^2$ is in the range for the skin effect to have an impact on the cable. Therefore, a design with stranded wires bundled instead of a solid conductor will be tested. The stranded coil model will be designed after the reference and be more similar to the real life model. This will be neglected for the FCJJ cable. This is because the size of the FCJJ conductor is smaller and the skin effect is much less pronounced in the cable [17].

4.8 Physics and multiphysics

The section explains the physics and multiphysics of the COMSOL setup and the importance of these interfaces. The physics implemented in this thesis is magnetic fields and heat transfer in solids, and the purpose is to calculate a specific set of equations and PDE. As a result, multiphysics depends on the results of physics and couples them together. Hence, the simulation conducted in this thesis uses electromagnetic heating as it couples the magnetic fields with transfer in solids.

4.8.1 Magnetic fields

In COMSOL, the simulation can be performed in the frequency domain. Thus, the derivative $\frac{\partial}{\partial_t}$ in the electric field (2.4) is replaced by the complex operator jw. Assuming the scalar potential effect is negligible, the simplified electric field can be written as:

$$\mathbf{E} = -j\omega\mathbf{A}. \tag{4.2}$$

The Maxwell equation is applied in this physics and is calculated with magnetic vector potential. Current is applied to the 3-phase cable with 120° phase shift for each phase. For the simulation to be completed these equations are solved: Faraday's law (4.2), Ampère's law (2.5) and Gauss's law (2.2). Thus, the total current density

can be expressed as:

$$\mathbf{J} = \sigma\mathbf{E} + j\omega\mathbf{D} + \sigma\mathbf{v} \times \mathbf{B} + \mathbf{J}_e. \tag{4.3}$$

Where $\mathbf{J}$ is the sum of four different currents. $\sigma\mathbf{E}$ is the conduction current, $j\omega\mathbf{D}$ is the displacement current, $\sigma\mathbf{v} \times \mathbf{B}$ is the motional current and $\mathbf{J}_e$ is the external current density.

Skin effect and eddy currents is simulated and will probably have an impact on the result. As a consequence, a design of the AXAL cable tries to mitigate the skin effect.
Lastly, this interface configures other electromagnetic properties for the metals and the cable. Linearized resistivity is one of those.

4.8.2 Heat transfer in solids

This interface governs the thermal behavior of the material, through thermal conduction. This allows placing heat sources, changing boundary conditions and material conditions to affect the radiation and convection. The temperature is solved with (2.6) Fourier's law, and the heat diffusion equation. Thermal behavior during the heating process is governed by the principle of energy conservation, which accounts for the transient temperature distribution, which results in heat conduction and generation [33]. For a solid medium, the general heat diffusion equation is implemented in COMSOL as:

$$\rho C_p \frac{\partial T}{\partial t} + \rho C_p \mathbf{u} \cdot \nabla T = \nabla \cdot (k \nabla T) + Q \tag{4.4}$$

where $\rho C_p \frac{\partial T}{\partial t}$ is the rate of change in internal energy of the material. ρ is the density and C_p is the specific heat capacity. $\rho C_p \mathbf{u} \cdot \nabla T$, the heat transport from the physical motion of the material and $\mathbf{u}$ being the velocity field.$\nabla \cdot (k \nabla T)$ describes the diffusion of heat and k is the thermal conductivity. Lastly, Q is electromagnetic losses. Air and ground temperature changes during the year. Thus, different heat sources are used to simulate the change in weather.

4.8.3 Electromagnetic heating

The coupling between the different physics interfaces is called induction heating and it starts with the magnetic field generating heat. Thus, the temperature increase alters the magnetic properties, the relative permeability $\mu(T)$, and the electrical conductivity $\sigma(T)$.

4.8.4 Heat source

Given the complex geometry of the AXAL cable design and the time consuming simulation, an approach with a simplified model was used. Therefore, a heat source model was developed only with heat transfer in solids and without magnetic field physics. This leaves out Electromagnetic Heating multiphysics, which couples the magnetic fields with the heating. Thus, a Heat source is added, which is affected by joule heating. Using the power loss (3.1), it can be defined as

$$Q_h = 0.5 \cdot \frac{J_z^2}{\sigma}. \tag{4.5}$$

In this implementation, the value of Qh will be the volumetric heating element generated from the current that flows through the conductor, Jz, the current density of the cross-area of the cable conductors, and the input current. 0.5 to convert the maximum current into the average power of AC and calculated from $(1/\sqrt{2})^2$ when simplifying the RMS value from Jz. Therefore, σ is the temperature dependent electrical conductivity, this is the implementation of linearized resistivity used in induction heating. Finally, the implementation of the Qh value in all the phases of the conductors is used as heat generation for the simulation.

4.9 Mesh

COMSOL utilizes FEM for solving the simulations, it is solved by breaking up the design into thousands of smaller pieces to calculate it step by step. This is possible when applying mesh. The mesh is a connection of many geometric shapes, often triangles, which follows the model's geometry, making it the bridge between the design and the mathematical solutions. With a more complex geometry design, the mesh will automatically higher, as shown in Figures 4.12. Higher mesh will result in higher complexity that results in longer simulation time. The preset finer mesh will be used for all simulations to get a realistic result without sacrificing time. With the same mesh preset the FCJJ cable is shown to have fewer mesh geometry and will have the shortest simulation time due to this. Comparing 4.12a and 4.12b for the AXAL cable, the stranded coil has a higher mesh count, over 80 % higher count, which has a large effect on the simulation time. The increased simulation time makes the stranded coil design impractical, and will not be used.

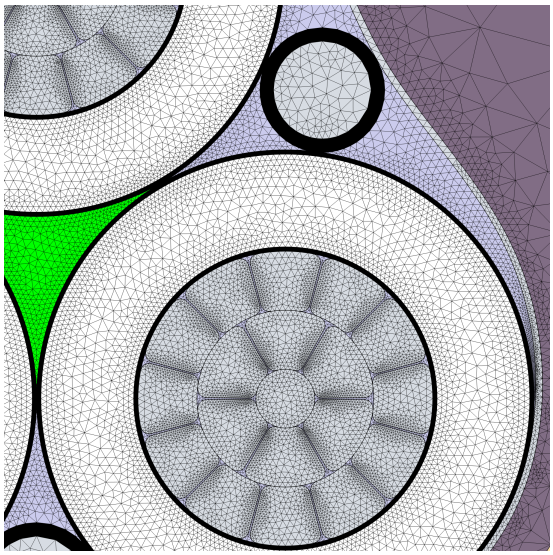

(a) The mesh of the stranded AXAL cable with induction heating design.

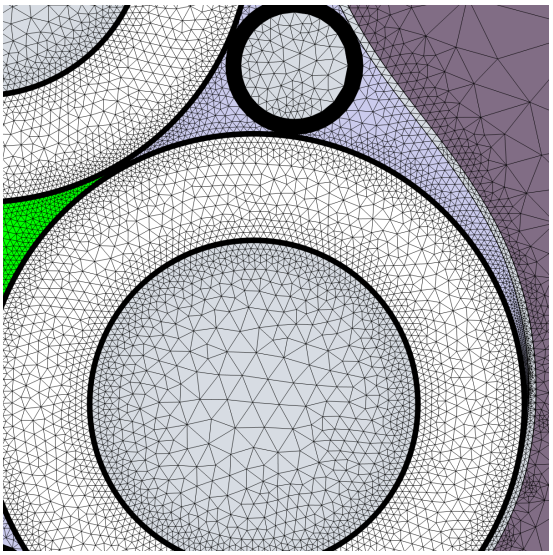

(b) The mesh of the AXAL cable with the heat source design.

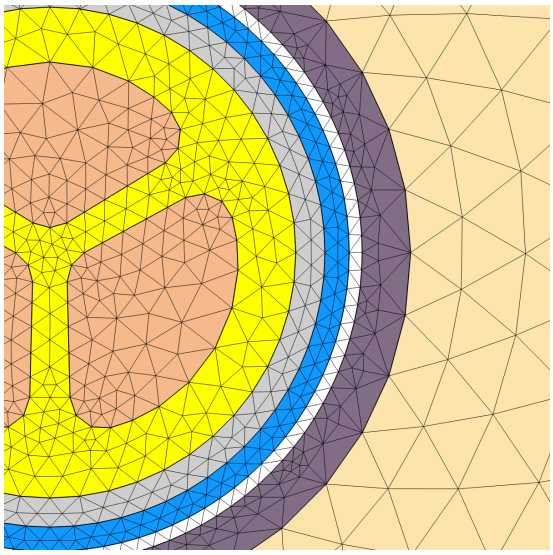

(c) The mesh of the FCJJ cable with induction heating design.

Figure 4.12: the mesh for the different simulations.

Adding more cables to the design is another factor that affects the complexity of the simulation, resulting in longer simulations. Figures 4.13 show that both the mesh are close to uniform outside the proximity of the cables. The three cable setup is close to three times the mesh count as the single cable. Similarly, the FCJJ cable has close to the same ratio between one and three cables, 2.5 times higher. Nevertheless, the total amount of mesh in FCJJ compared to AXAL is considerably less, making the simulation time of all different copper cable in the similar range.

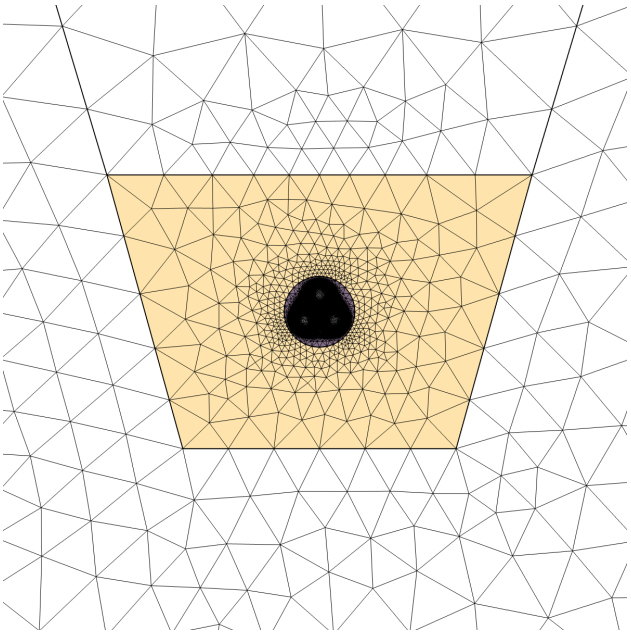

(a) Meshing of the AXAL cable design.

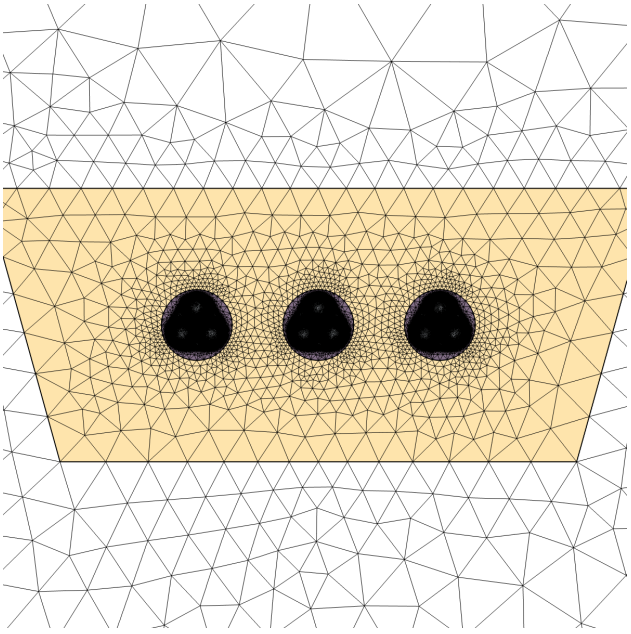

(b) Meshing of the three cables AXAL design.

Figure 4.13: Comparing the mesh with more cables.

4.10 Frequency–Transient Study

To accurately model the system's behavior, a Frequency–Transient study was selected. This approach involves both the frequency and time domain and solves the physics for the different timescales. The magnetic fields are solved in the frequency domain to obtain the electromagnetic losses and the heat transfer is solved in the time domain for temperature.

To ensure that the simulation has a realistic initial condition, a warm-up phase of 800 hours is implemented. This makes sure that it reaches steady-state temperature. This study steps hourly, in total over 9500 times. Overall, the simulation is run for a year of measured current data, and the extra 800 h data at the beginning are omitted from the results.
Lastly, with the simulation finished, the hourly temperature results are exported to figures and excel spreadsheets.

4.11 Implementation of Arrhenius equation

To quantify the thermal degradation of power cables, the project implements the Arrhenius equations (2.7), (2.10) to assess the thermal aging. This methodology incorporates the time dependent temperatures from the COMSOL simulations and evaluates the thermal stress on the material. Furthermore, MATLAB is used for the calculations in the section.

Since the simulation calculates two cables models, different values for E_a and T_{ref} are applied. The FCJJ cable with oil-impregnated paper insulation has a rated temperature of 65 ° C and an activation energy of $1.1eV$[34]. The AXAL with XLPE insulation cable insulation has a rated temperature of 90 ° C and activation energy of $1.287eV$ from [35]. Hence, T is the simulated temperature value of the cable and the Boltzmann constant k_B is known. The relative aging factor V can be obtained. Applying V and Δt to the (2.11) integration can be calculated. Lastly, the calculation of (2.10) and (2.11) for all the simulated values and the aging of the material can be obtained.

5
Simulation Results

The results from the COMSOL simulation for both FCJJ and AXAL cables are presented in this chapter. In sections 5.1 and 5.2, when referring to an increase in temperature, the reference point is the configuration of one cable under normal conditions, for the said cable. The graphs for the temperature profiles show the highest value of the temperature in the cable at any given time, and it is in the conductor and the insulation. As mentioned in section 4.6, for the multiple cable configurations, the cables will have different results. However, this work will focus on the cable with the highest load. In figure 5.1 the average temperature of the air during the year is shown, this is used for all simulations.

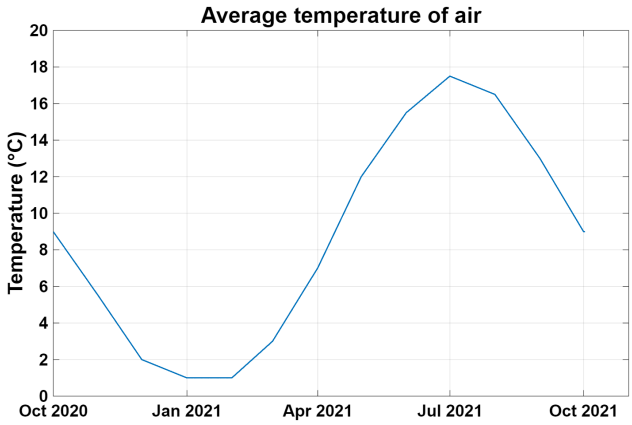

Figure 5.1: Average temperature of the air used for all the simulations.

5.1 FCJJ cable

5.1.1 One cable

For the magnetic flux plot, figure 5.2a shows that the field is the strongest between the conductors and it decreases further out. Similarly, the temperature plot shows the same behavior according to figure 5.2b.

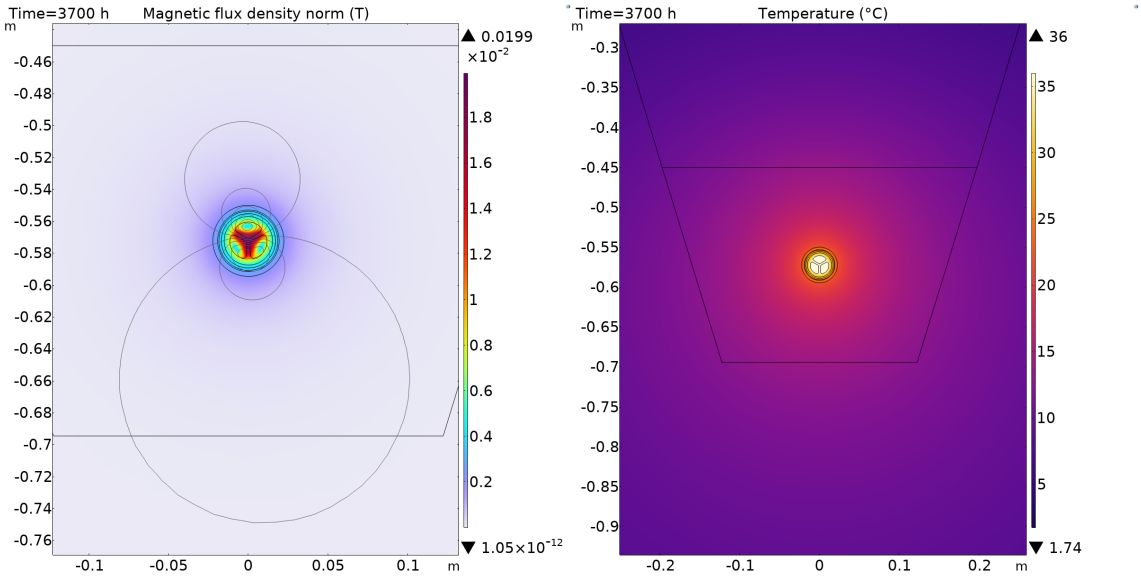

(a) The magnetic flux of the FCJJ cable at a specific time.

(b) The temperature of the FCJJ cable and the surrounding area at a specific time.

Figure 5.2: Magentic flux and temperature of the FCJJ cable.

Figure 5.3 show 3 simulation results, one during normal condition, one when the soil is drying and the last is when the soil has dried. 5.3a and 5.3b are the only simulations that do not have their peaks during the winter periods, even if their relatively close. This is due to the temperature from the load not being high enough and the temperature of the ground being proportionately high during summer periods.
As shown in figure 5.3b and 5.3c, the cable temperature is 7% and 38% higher for the respective two soil scenarios with lower thermal conductivity. The maximum temperature is still well within the cable's rated temperature.

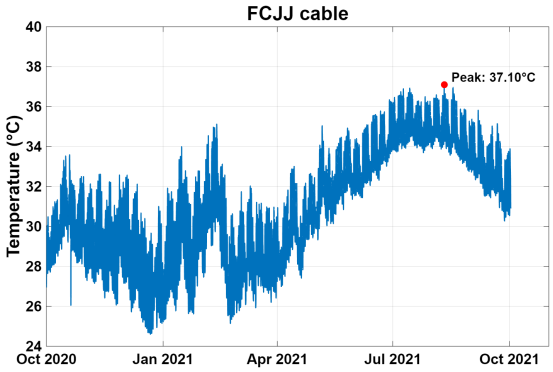

(a) Temperature plot of one FCJJ cable during normal condition over a year.

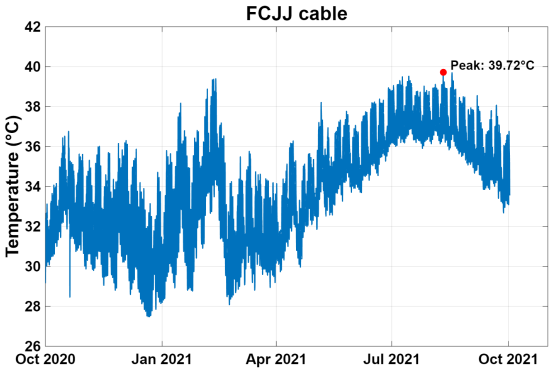

(b) Temperature plot of one FCJJ cable over a year when the surrounding soil is drying.

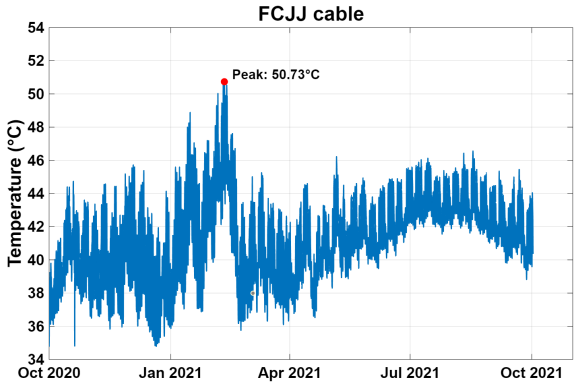

(c) Temperature plot of one FCJJ cable over a year when the surrounding soil is completely dried.

Figure 5.3: These graphs plots the highest temperature in the simulation, inside the cable's and insulation.

5.1.2 Two cables

The cable with the highest temperature is still the same cable with the same load as the cable shown in figure 5.2. From the results shown in figures 5.4, the temperature has increased. Both the magnetic flux and the temperature get affected by the addition of a second cable. With flux, it still has the same peak between the conductors, but the magnetic fields of the two cables influence each outer. The temperature is increased, both inside the cable and the surrounding soil. It radiates further and has a higher temperature.

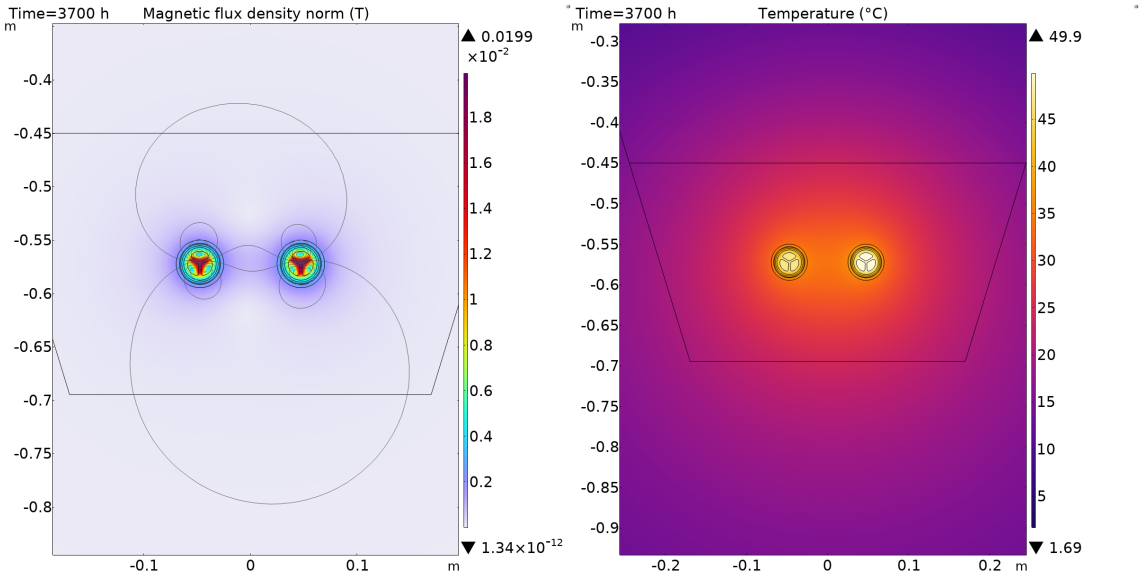

(a) The magnetic flux of two FCJJ cables at a specific time.

(b) The temperature of two FCJJ cables and the surrounding area at a specific time.

Figure 5.4: The result with two FCJJ cables.

Furthermore, compared to the first simulation 5.3a, the simulation with two cables increases the maximum temperature by 25% in 5.5a, 41% in 5.5b with the scenario of the drying soil and 84% in 5.5c, when the soil is dried. This is for one of the cables because the second cable has a lower load. The overall temperature values are still far below the rated temperature for the first two scenarios, but the last with the dried soil, it exceeds the rated temperature.

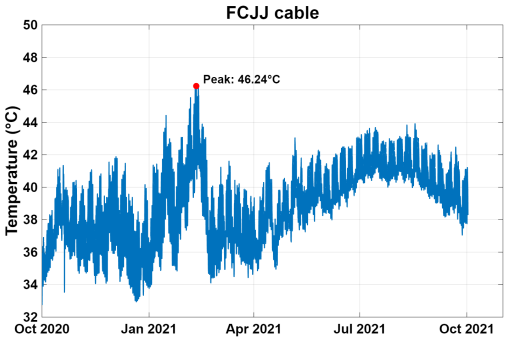

(a) Temperature plot of two FCJJ cables during normal condition over a year.

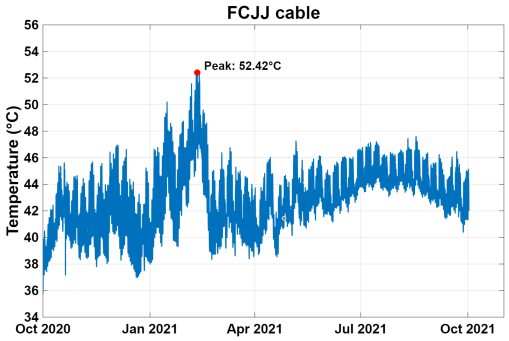

(b) Temperature plot of two FCJJ cables over a year when the surrounding soil is drying.

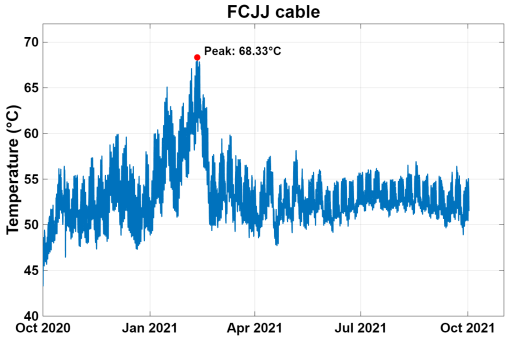

(c) Temperature plot of two FCJJ cables over a year when the surrounding soil is completely dried.

Figure 5.5: These graphs plots the highest temperature in the simulation, inside the cable's conductors and insulation.

5.1.3 Three cables

With the addition of a cable to the right, similar to the two cable configuration, the existing cables will have the same load. The model with three cables is the simulation that replicates a real scenario. Hence, more focus will be on this setup. As a result of a third cable, the temperature increases in the conductors, shown in figure 5.6b. Similarly with two cables, the temperature increases and radiates further. There are now higher local spikes between the cables. The magnetic flux does not change as drastically compared to the two cables shown in figure 5.4a. Figure 5.6a shows that all cables influence each other and the highest flux exists between the phases of each cable.

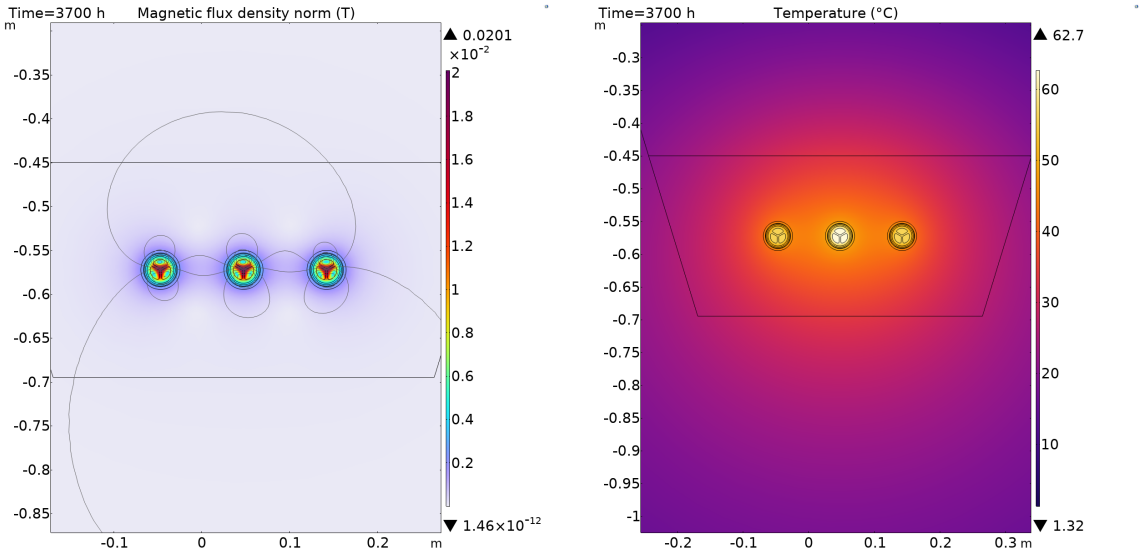

(a) The magnetic flux of three FCJJ cables at a specific time.

(b) The temperature of three FCJJ cables and the surrounding area at a specific time.

Figure 5.6: The result with three FCJJ cables.

Four different scenarios simulated, normal condition 5.7a, the peak with 10% higher current 5.7c and the two drying soil scenarios, 5.7b, 5.7d. As a result of the simulations, the maximum temperature has increased close to 57%, 93%, 79% and 136% in the order as mentioned before. This yields three simulation over the rated temperature of 65 °C for oil-impregnated paper in steady-state conditions.

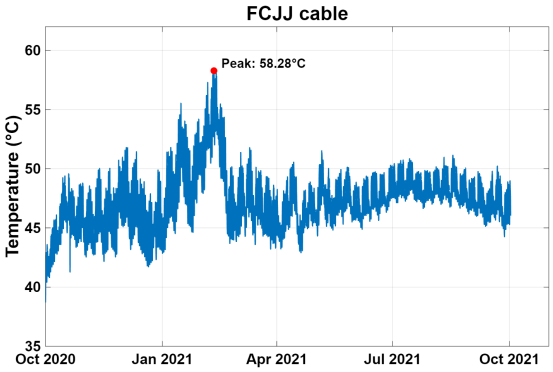

(a) Temperature plot of three FCJJ cables during normal condition over a year.

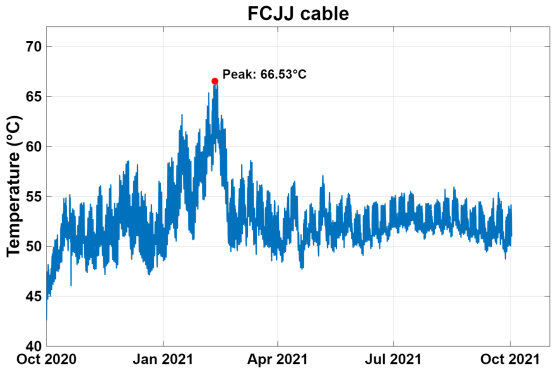

(b) Temperature plot of three FCJJ cables over a year when the surrounding soil is drying.

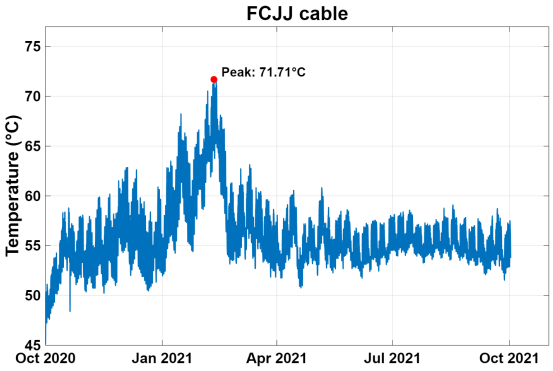

(c) Temperature plot of three FCJJ cables over a year when the peak has increased with 10 percent.

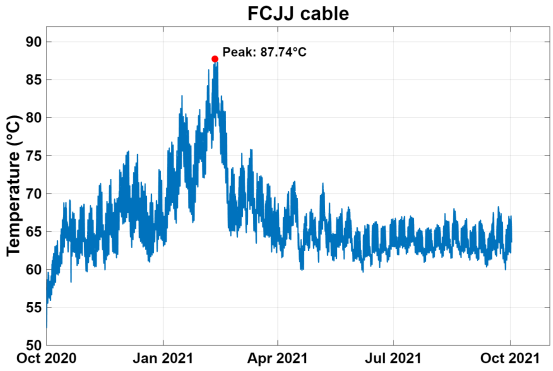

(d) Temperature plot of three FCJJ cables over a year when the surrounding soil has completely dried.

Figure 5.7: These graphs plots the highest temperature in the simulation, inside the cable's conductors and insulation.

5.2 AXAL cable

5.2.1 one cable

Only one simulation with induction heating for the AXAL cable is conducted, figures 5.8 and 5.9a illustrate the results. Comparing the temperature with the induction heating model, the heat source model in figure 5.9b shows similar results. Furthermore, rest of the simulations is with the heat source model which follow the same methodology as the FCJJ configurations.

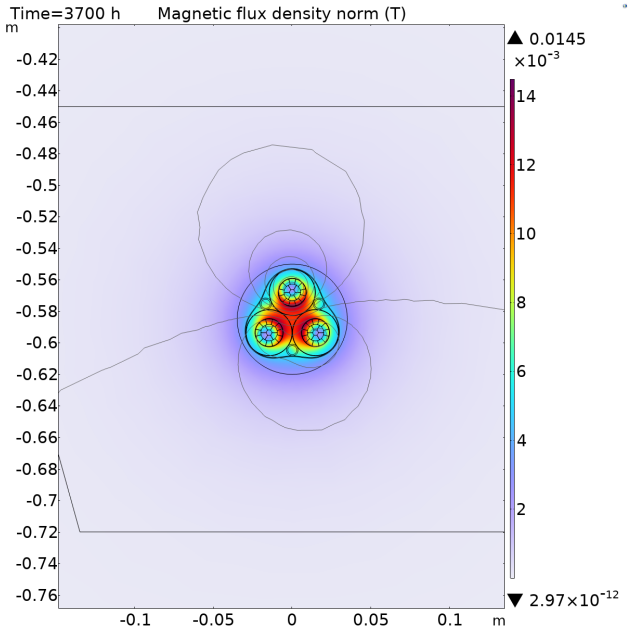

Figure 5.8: The magnetic flux of the AXAL cable at a specific time.

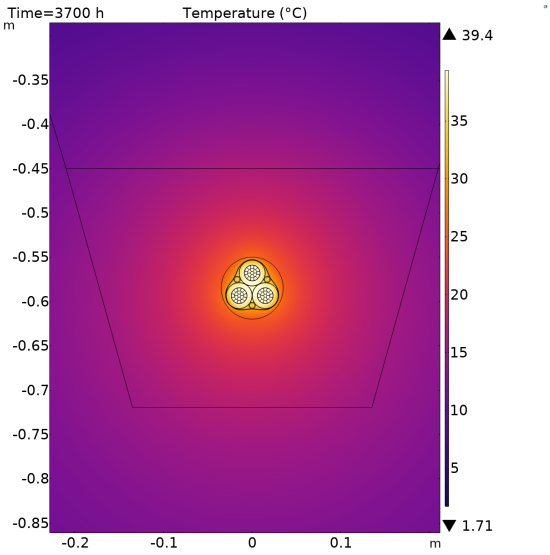

(a) The temperature of the AXAL cable and the surrounding area at a specific time with the induction heating simulation.

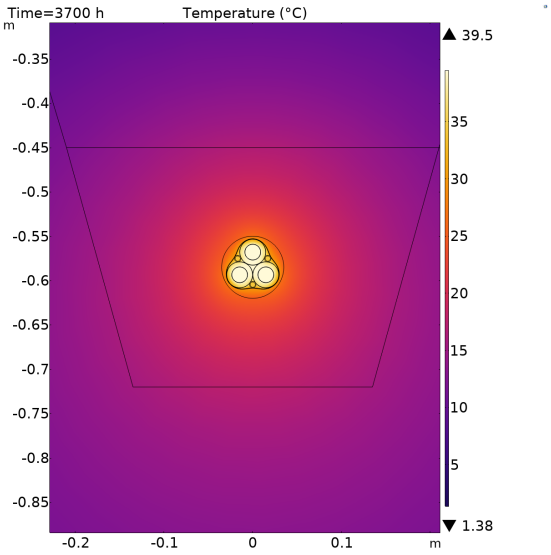

(b) The temperature of the AXAL cable and the surrounding area at a specific time with the heat source simulation.

Figure 5.9: The result of the AXAL cable.

The plots of the different simulations, induction heating and heat source show values that are similar with figures 5.10a and 5.10b. The stranded design has a slightly higher temperature profile, this could be due to more eddy current losses with the magnetic field model. Nevertheless, the different models gives close to similar results. As a result of the drying of soil simulation, as figure 5.10c, the temperature

increases by 8% and the completely dried soil scenario in figure 5.10d increased the temperature by 40%. However, there is considerable margin to the rated temperature.

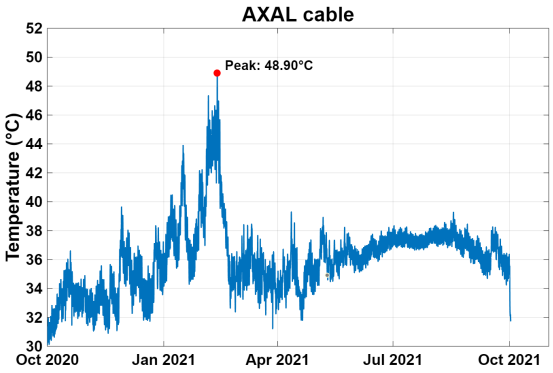

(a) Temperature plot of one AXAL cable during normal condition over a year with the heat source simulation.

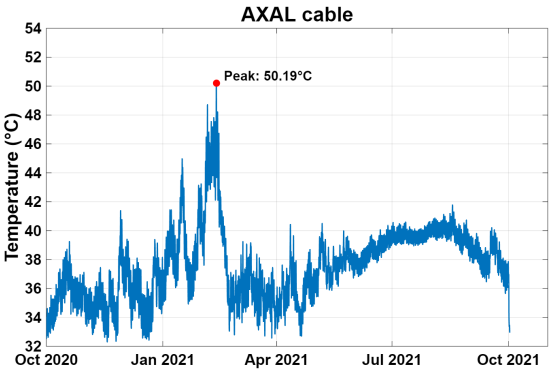

(b) Temperature plot of one AXAL cable during normal condition over a year with the induction heating simulation.

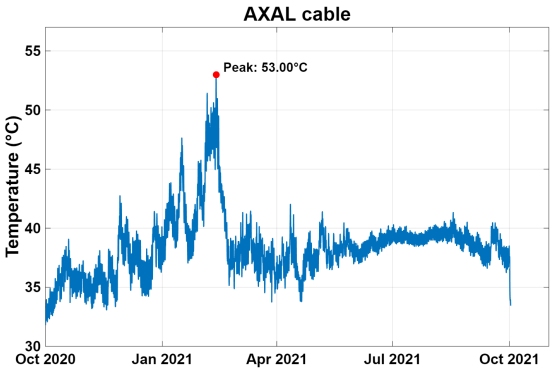

(c) Temperature plot of one AXAL cable over a year when the surrounding soil is drying, with the heat source simulation.

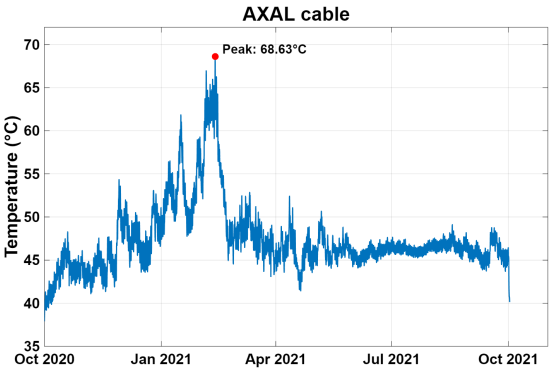

(d) Temperature plot of one AXAL cable over a year when the surrounding soil is completely dried, with the heat source simulation.

Figure 5.10: These graphs plots the highest temperature in the simulation, inside the cable's conductors and insulation.

5.2.2 Two cables

The second cable simulation gives a higher overall temperature and higher ambient temperature that radiates further, as shown in figures 5.11 and 5.12a. The cable on the right is the same cable with the same load as the simulation of one cable in figure 5.9b. This cable has the highest load in the simulation and results in the highest temperature.

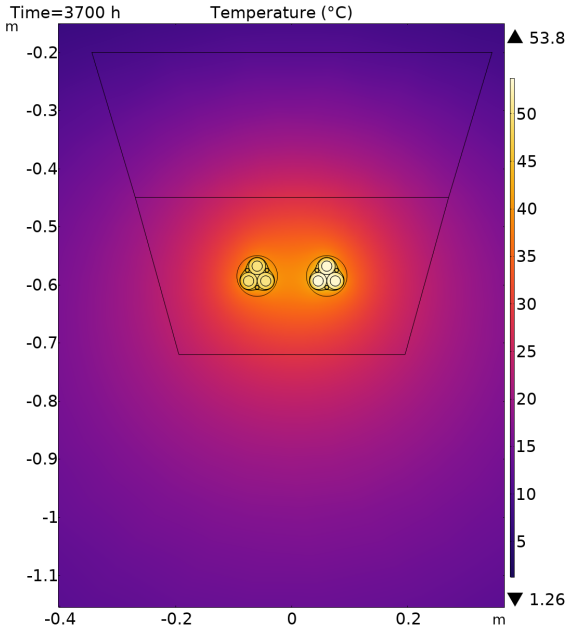

Figure 5.11: The temperature of two AXAL cables and the surrounding area at a specific time with the heat source simulation.

Hence, as shown in figure 5.12a, 5.12b and 5.12c, the peak temperature values increased with close to 41% during normal conditions, 46% when the surrounding soil is drying and 94% for the dried soil, when compared to the first cable, 5.10a. The last scenario exceeded the rated temperature, with the other, there is still a sufficient margin to the rated temperature.

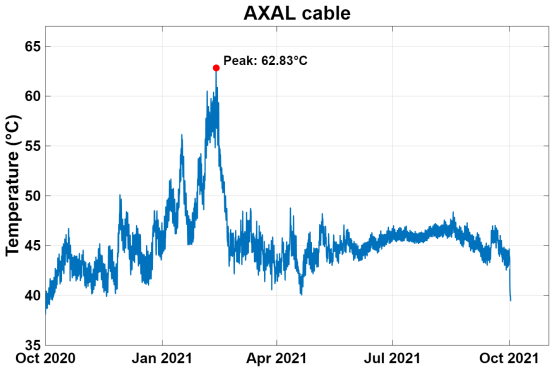

(a) Temperature plot of two AXAL cables during normal condition over a year with the heat source simulation.

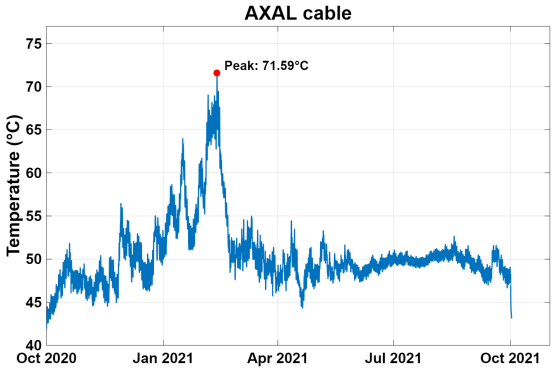

(b) Temperature plot of two AXAL cables over a year when the surrounding soil is drying, with the heat source simulation.

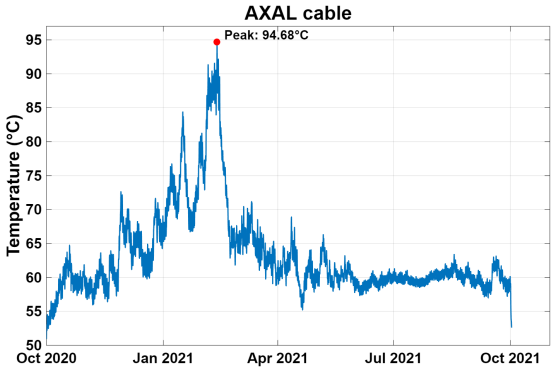

(c) Temperature plot of two FCJJ cables over a year when the surrounding soil is completely dried.

Figure 5.12: These graphs plots the highest temperature in the simulation, inside the cable's conductors and insulation.

5.2.3 Three cables

A third cable is added to the right and has a different load. The other two cables are still the same load as in the simulation shown in figure 5.11. The middle cable has the same load and will have the highest temperature, as shown in figure 5.13. Similarly to the FCJJ design, the AXAL three cable model for normal condition is designed after a real life situation. Figure 5.13 shows with the addition of a third cable, the temperature increases and the ambient temperature radiates further. Figures 5.13 and 5.14a show a similar observation.

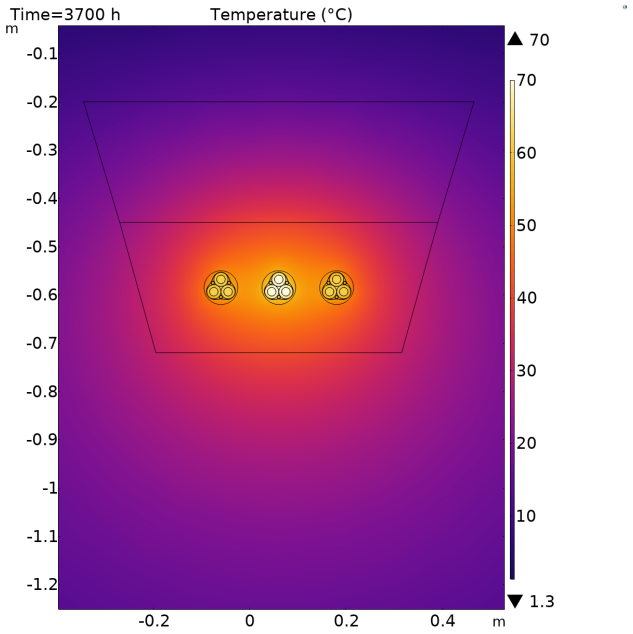

Figure 5.13: The temperature of three AXAL cables and the surrounding area at a specific time with the heat source simulation.

Four different scenarios were simulated, 1) normal condition as in 5.14a, 2) the soil drying out as in 5.14b, 3) the peak with 10% higher peak 5.14c and 4) when the soil has completely dried out as in 5.14d. As a result, the maximum temperature has increased close to 66%, 90%, 113%, and 156% in the order mentioned earlier. This yields three simulations at the rated temperature of 90 °C for XLPE and over a considerable period of time.

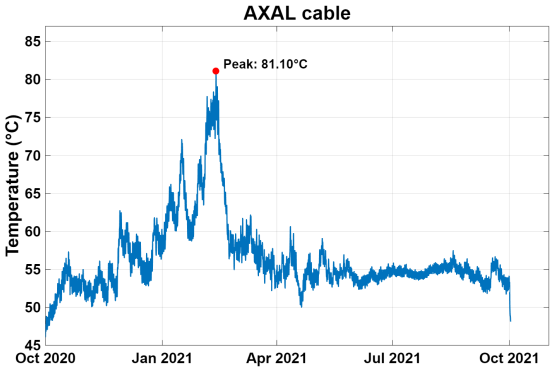

(a) Temperature plot of three AXAL cables during normal condition over a year with the heat source simulation.

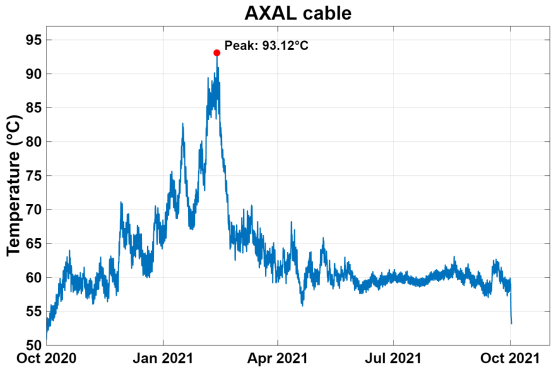

(b) Temperature plot of three AXAL cables over a year when the surrounding soil is drying out, with the heat source simulation.

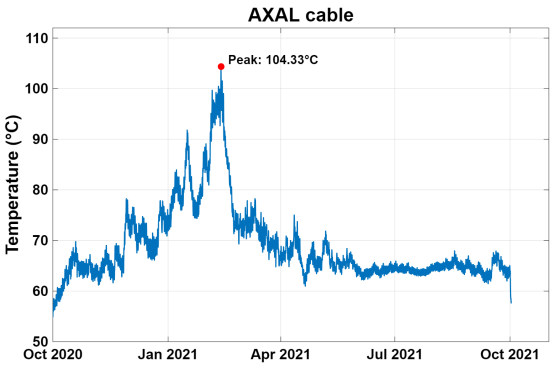

(c) Temperature plot of three AXAL cables over a year when the peak has increased with 10 percent, with the heat source simulation.

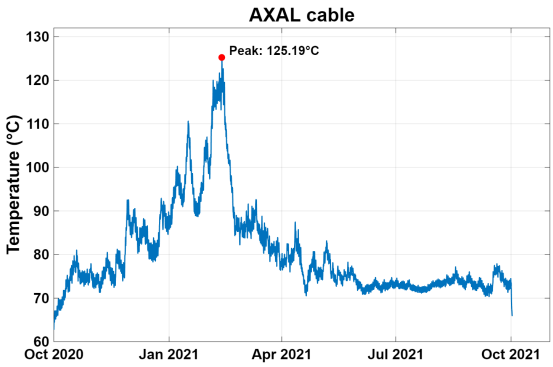

(d) Temperature plot of three AXAL cables over a year when the surrounding soil has dried completely, with the heat source simulation.

Figure 5.14: These graphs plots the highest temperature in the simulation, inside the cable's conductors and insulation.

5.3 Arrhenius results

First, with Arrhenius equation (2.10), cable aging was obtained. Simulations well below the rated temperature showed that the thermal stress have been negligible. As a result, only the aging in the simulations with three cables and one two cable scenario with the dried soil were evaluated with the Arrhenius equation. The results have shown that the conductor and the insulation temperature are equivalent for all the simulations. Thus, the maximum temperature of the cable is for both materials. However, for the thesis and for calculating the thermal aging, the insulation is in focus.
Simulation results when the soil is completely dried for the two cables configuration, are shown in table 5.1 and figure 5.15. The FCJJ cables exceed the thermal rating. As a result, the highest peak reaches 68.33 °C, and at the highest thermal stress the material degrades 1.45 times faster than normal. The total time over the thermal rating is 3 days and the equivalent aging is equal to 0.29 years, 105 days after a whole year

Table 5.1: Values from the Arrhenius equation calculations for FCJJ cable.

FCJJ Paper/oil insulation		Unit		Simplified unit
Peak temperature	68.33	°C		
Max aging factor	1.45			
Overheating duration	73	Hours	3	Days
Equivalent aging	0.2877	Years	105	Days

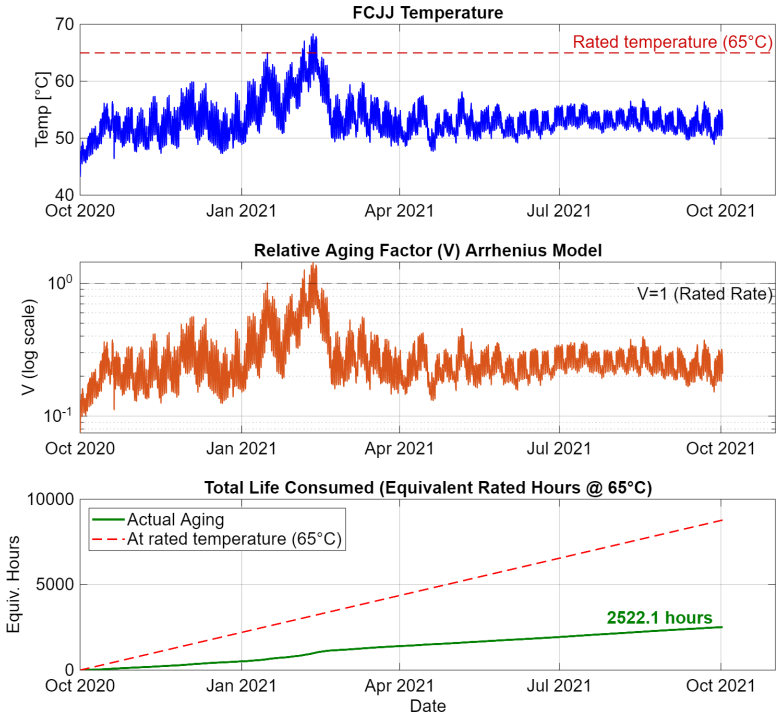

Figure 5.15: Aging of the two FCJJ cable setup during the one year period when the soil has completely dried.

For the two cable AXAL model when the soil has completely dried, shown with table 5.2 and figure 5.16, gives a similar result to the FCJJ version. The AXAL cables exceed the thermal rating. As a result, the highest peak reaches close to 195 °C, and at the highest thermal stress, the material degrades 1.7 times faster than normal. The total time over the thermal rating is 29 hours, and the equivalent aging is equal to 25 days after a whole year.

Table 5.2: Values from the Arrhenius equation calculations for AXAL cable.

AXAL XLPE insulation		Unit		Simplified unit
Peak temperature	94.68	°C		
Max aging factor	1.7			
Overheating duration	29	Hours	1.21	Days
Equivalent aging	0.0674	Years	25	Days

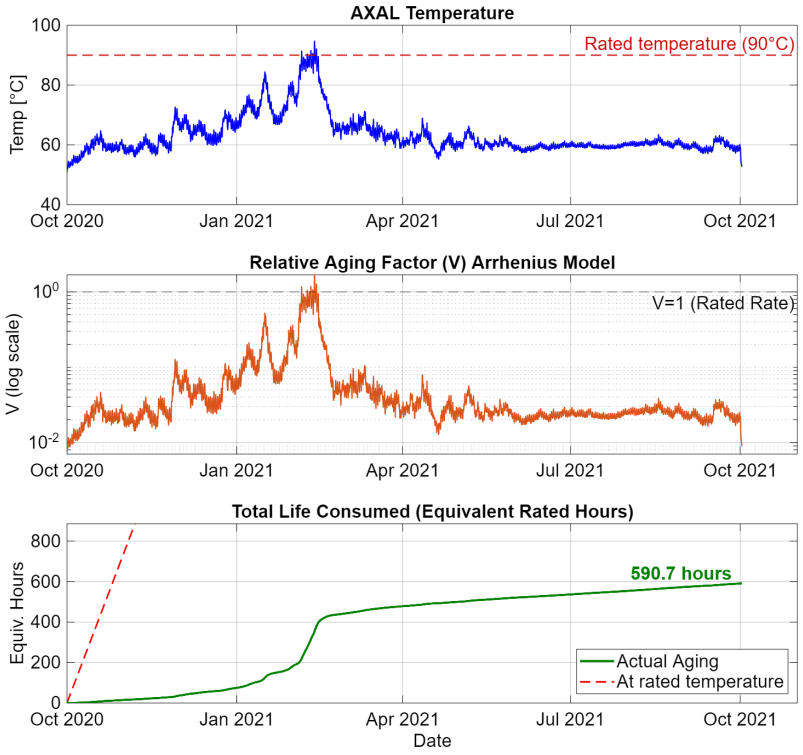

Figure 5.16: Aging of the two AXAL cable setup during the one year period when the soil has completely dried.

Table 5.3 and figure 5.17, show the aging from the three FCJJ cables configuration under normal condition. Thermal rating is never reached and the equivalent aging equals to 0.13 years, almost 48 days after a whole year.

Table 5.3: Values from the Arrhenius equation calculations for FCJJ cable.

FCJJ Paper/oil insulation		Unit	Simplified unit	
Peak temperature	58.3	°C		
Max aging factor	0.47			
Overheating duration	0	Hours		
Equivalent aging	0.13	Years	47.5	Days

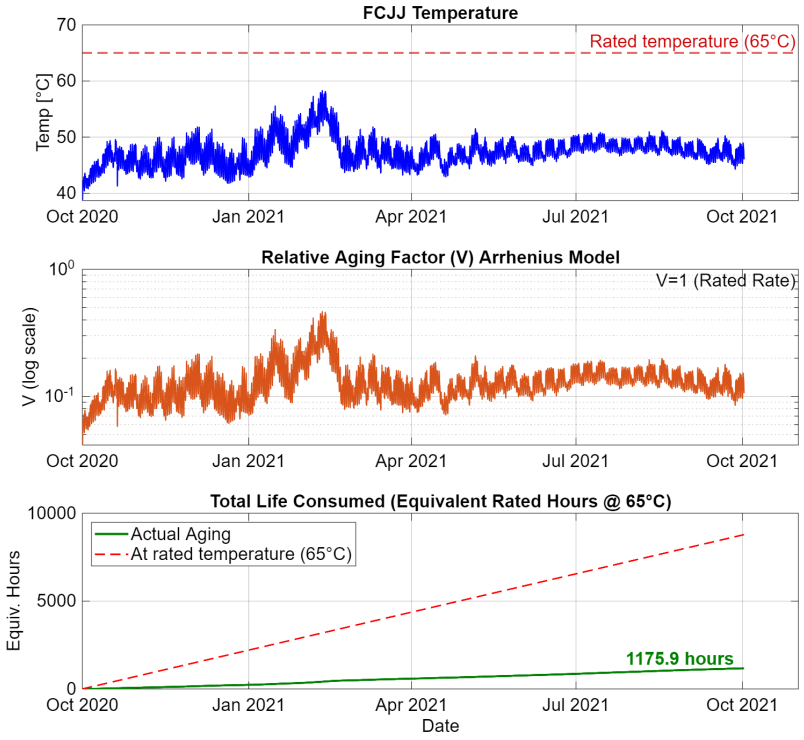

Figure 5.17: Aging of the FCJJ cable during the one year period.

Table 5.4 and figure 5.18, shows the aging from the three AXAL cables configuration under normal condition. Thermal rating is never reached and the equivalent aging equals to 0.0211 years, almost 8 days after a whole year.

Table 5.4: Values from the Arrhenius equation calculations for AXAL cable.

AXAL XLPE insulation		Unit	Simplified unit	
Peak temperature	81.1	°C		
Max aging factor	0.37			
Overheating duration	0	Hours		
Equivalent aging	0.0211	Years	7.7	Days

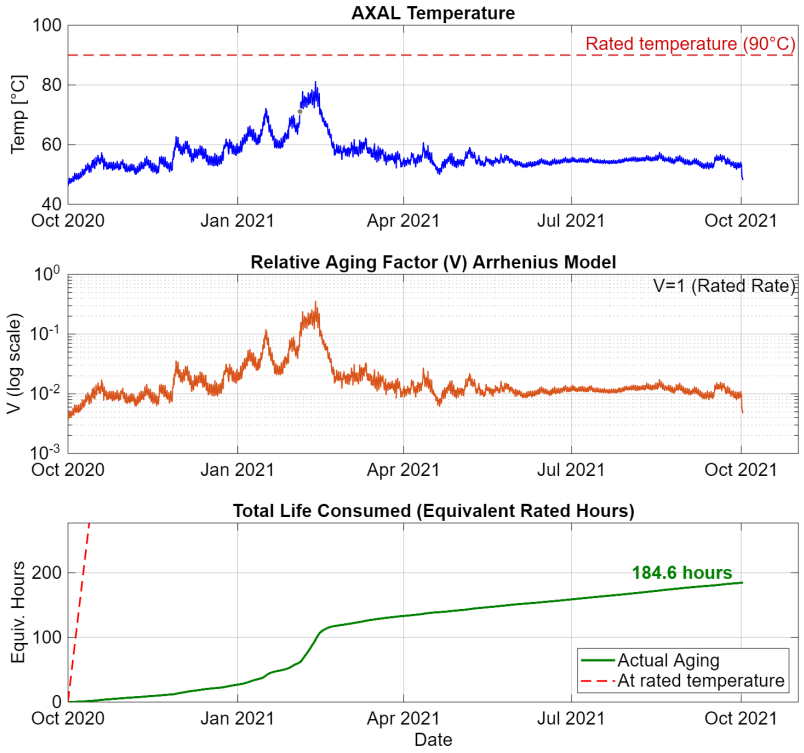

Figure 5.18: Aging of the AXAL cable during the one year period.

Table 5.5 and figure 5.19 show the aging values from the three cables FCJJ simulation when the soil is drying. This simulation is the first of the three FCJJ cable setup that exceeds the thermal rating with a peak temperature close to 67 °C. As a result, at the highest thermal stress, the material degrades 1.19 times faster than it was designed. The total time over the thermal rating is 37 days, and the equivalent aging is equal to 0.26 years, 95 days after a whole year.

Table 5.5: Values from the Arrhenius equation calculations for FCJJ cable with the soil drying.

FCJJ Paper/oil insulation		Unit		Simplified unit
Peak temperature	66.53	°C		
Max ageing factor	1.19			
Overheating duration	27	Hours	1.125	Days
Equivalent aging	0.26	Years	95	Days

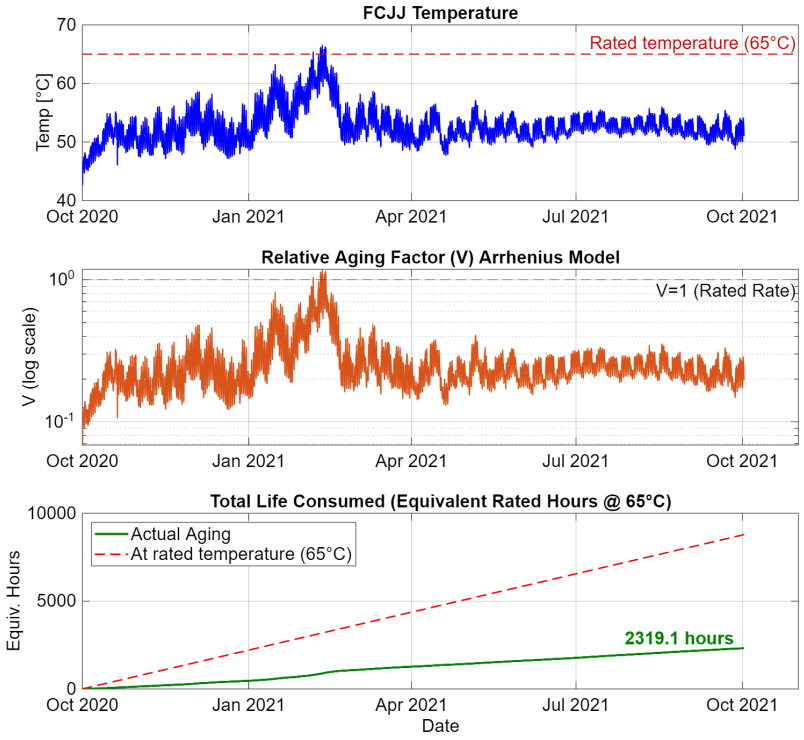

Figure 5.19: Aging of the FCJJ cable during the one year period with the soil drying.

Similarly as in the case with FCJJ cables, the three AXAL simulation when the soil is drying is the first of three AXAL cable setup that exceeds the thermal rating, as shown in table 5.6 and figure 5.20. Thus, peak temperatures close to 93 °C and at the highest thermal stress the material degrades 1.42 times faster than it was constructed for. The total time over the thermal rating is 11 hours, and the equivalent aging is equal to 0.063 years, 23 days after a whole year.

Table 5.6: Values from the Arrhenius equation calculations for AXAL cable with the soil drying.

AXAL XLPE insulation		Unit		Simplified unit
Peak temperature	93.12	°C		
Max aging factor	1.42			
Overheating duration	11	Hours	0.46	Days
Equivalent aging	0.063	Years	23	Days

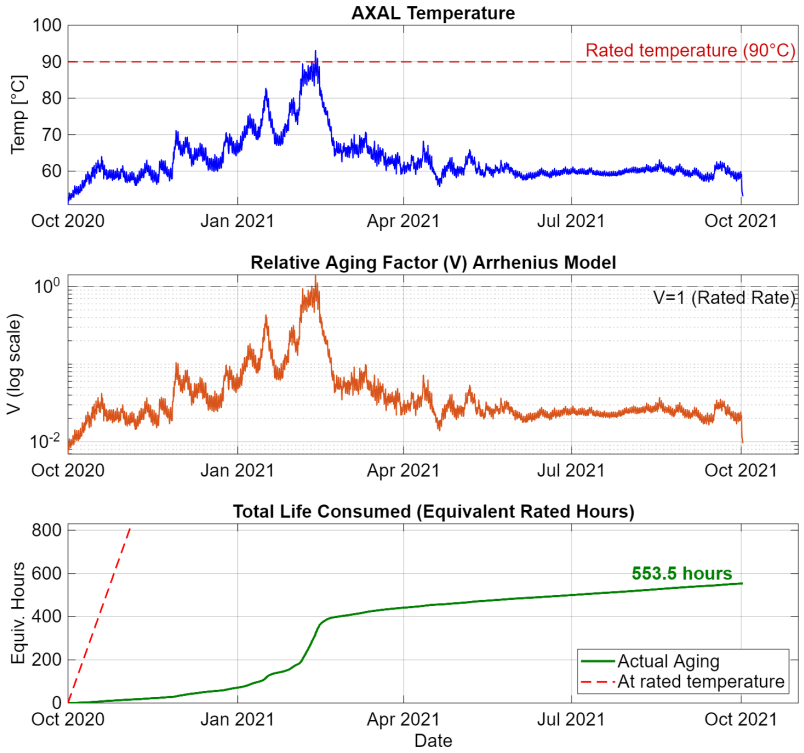

Figure 5.20: Aging of the AXAL cable during the one year period with the soil drying.

A higher peak current is simulated and the results are summarized in table 5.7 and shown in figure 5.21. FCJJ cables exceed the thermal rating on multiple occasions with the highest peak close to 72 °C, and at the highest thermal stress the material degrades 2.1 times faster than that constructed for. The total time over the thermal rating is 12 days and the equivalent aging equals to 0.4 years, 147 days after a whole year.

Table 5.7: Values from the Arrhenius equation calculations for FCJJ cable with a 10% higher peak.

FCJJ Paper/oil insulation		Unit		Simplified unit
Peak temperature	71.71	°C		
Max aging factor	2.1			
Overheating duration	282	Hours	11.75	Days
Equivalent aging	0.4	Years	147	Days

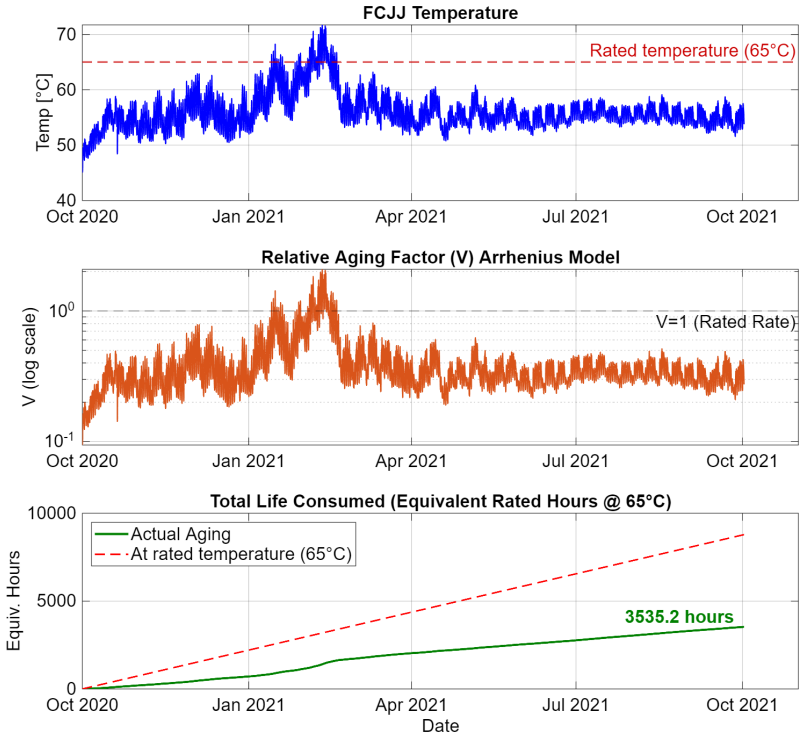

Figure 5.21: Aging of the FCJJ cable during the one year period with a 10% higher peak.

In the case of the AXAL simulation with the highest peak current, Table 5.8 and figure 5.22 shows cables exceeding the thermal rating on multiple separate instances. As a result, the highest peak reaches 104 °C, and at the highest thermal stress the material degrades 4.8 times faster than normal. The total time over the thermal rating is 12 days, and the equivalent aging is equal to 0.163 years, 59.5 days after a whole year.

Table 5.8: Values from the Arrhenius equation calculations for AXAL cable with a 10% higher peak.

AXAL XLPE insulation		Unit		Simplified unit
Peak temperature	104.33	°C		
Max aging factor	4.8			
Overheating duration	291	Hours	12.125	Days
Equivalent aging	0.163	Years	59.5	Days

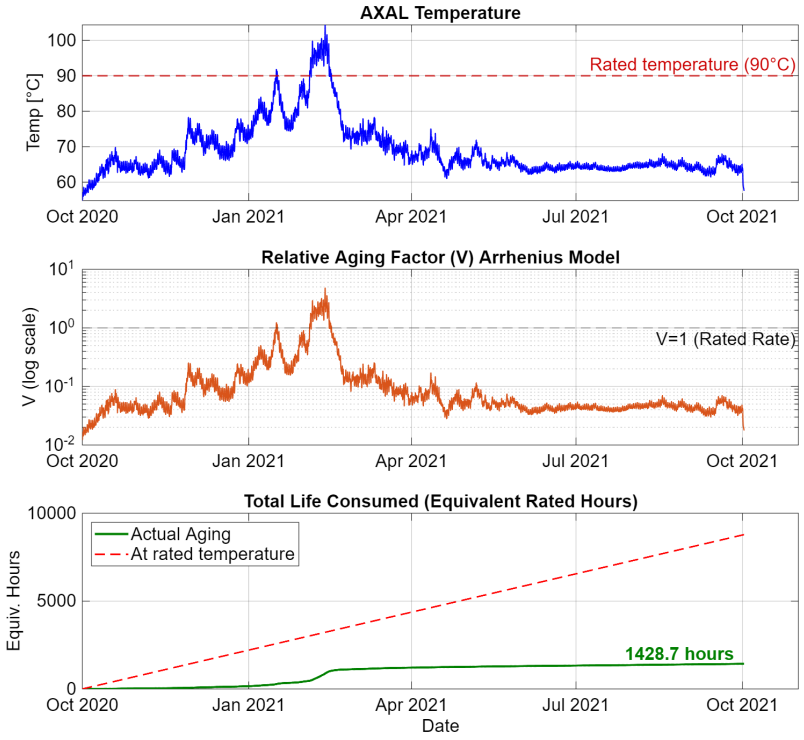

Figure 5.22: Aging of the AXAL cable during the one year period with a 10 percent higher peak.

In the end, simulation results when the soil is completely dried, are shown in table 5.9 and figure 5.23. The FCJJ cables exceed the thermal rating multiple times and are remarkably long periods of time. As a result, the highest peak reaches 87.7 °C, and at the highest thermal stress the material degrades 10.8 times faster than normal. The total time over the thermal rating is 202 days and the equivalent aging is equal to 1.42 years, 517 days after a whole year

Table 5.9: Values from the Arrhenius equation calculations for FCJJ cable when the soil has completely dried.

FCJJ Paper/oil insulation		Unit		Simplified unit
Peak temperature	87.7	°C		
Max aging factor	10.8			
Overheating duration	4844	Hours	202	Days
Equivalent aging	1.4158	Years	517	Days

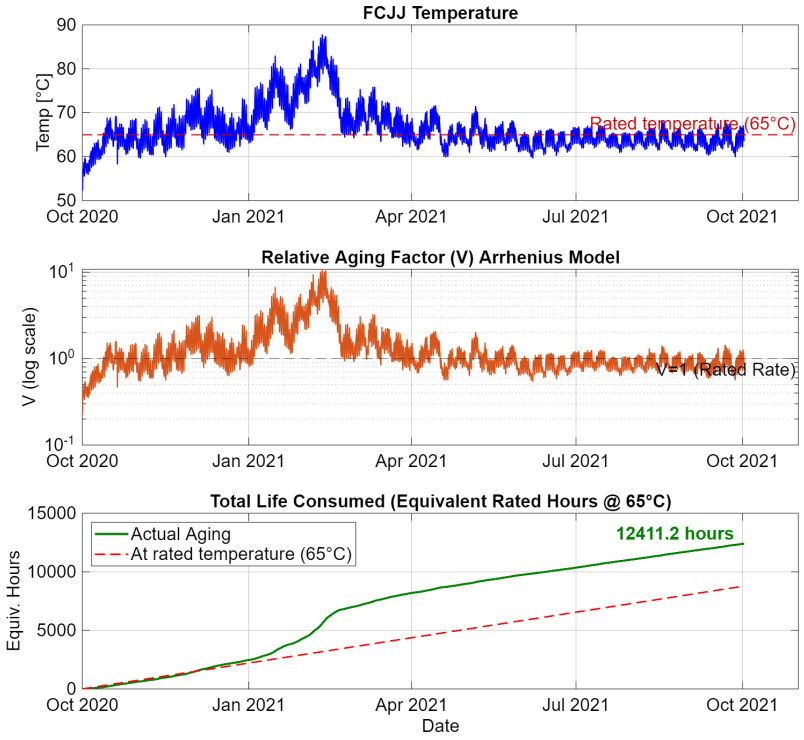

Figure 5.23: Aging of the FCJJ cable during the one year period when the soil has completely dried.

The simulation of the AXAL model when the soil has completely dried, shown with table 5.10 and figure 5.24, gives a similar result to the FCJJ version. The AXAL cables exceed the thermal rating several times, one of which being a very long period. As a result, the highest peak reaches close to 125 °C, and at the highest thermal stress, the material degrades 37.8 times faster than normal. The total time over the thermal rating is 52 days, and the equivalent aging is equal to 1.04 years, 380 days after a whole year.

Table 5.10: Values from the Arrhenius equation calculations for AXAL cable when the soil has completely dried.

AXAL XLPE insulation		Unit		Simplified unit
Peak temperature	125.2	°C		
Max aging factor	37.8			
Overheating duration	1245	Hours	52	Days
Equivalent aging	1.04	Years	380	Days

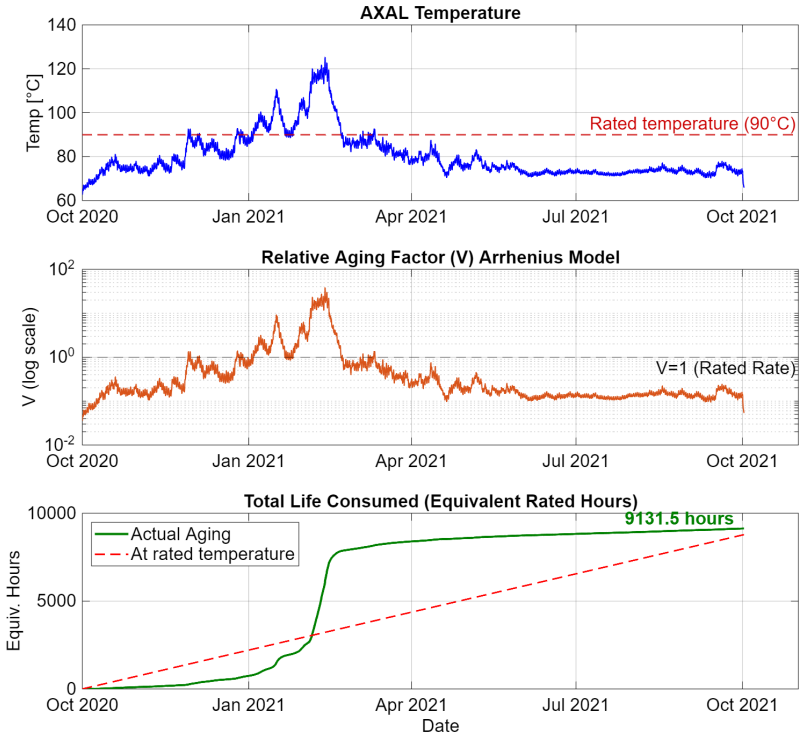

Figure 5.24: Aging of the AXAL cable during the one year period when the soil has completely dried.

5.3.1 Overall thermal aging

The thermal aging is calculated for the insulation materials of both cables for various temperature profiles. As summarized in table 5.11, the result shows the relative aging with respect to the case when the temperature was kept at rated value over a year. The AXAL cable would theoretically age over more than 59 years if kept at 130°C. As a result, the aging increases exponentially when operating above the rated temperature.

Table 5.11: Thermal aging for AXAL and FCJJ cables at various temperatures.

AXAL		FCJJ	
Temperature °C	**Aging years**	**Temperature °C**	**Aging years**
70	0.091	40	0.049
80	0.312	50	0.17
85	0.563	60	0.568
90	1	65	1
95	1.7479	70	1.74
100	3.01	75	2.96
110	8.56	80	4.98
130	59.2	90	13.47
150	340	105	54.3

5.4 Sensitivity analysis

To evaluate the robustness of the findings and to identify the critical parameters of the simulation, a sensitivity analysis was carried out. This analysis verifies that the conclusions drawn in this thesis are not excessively reliant on a specific assumption of a parameter.
A series of simulations were conducted for both cables to evaluate thermal robustness. Thus, figures 5.25 and 5.26 illustrate the results.

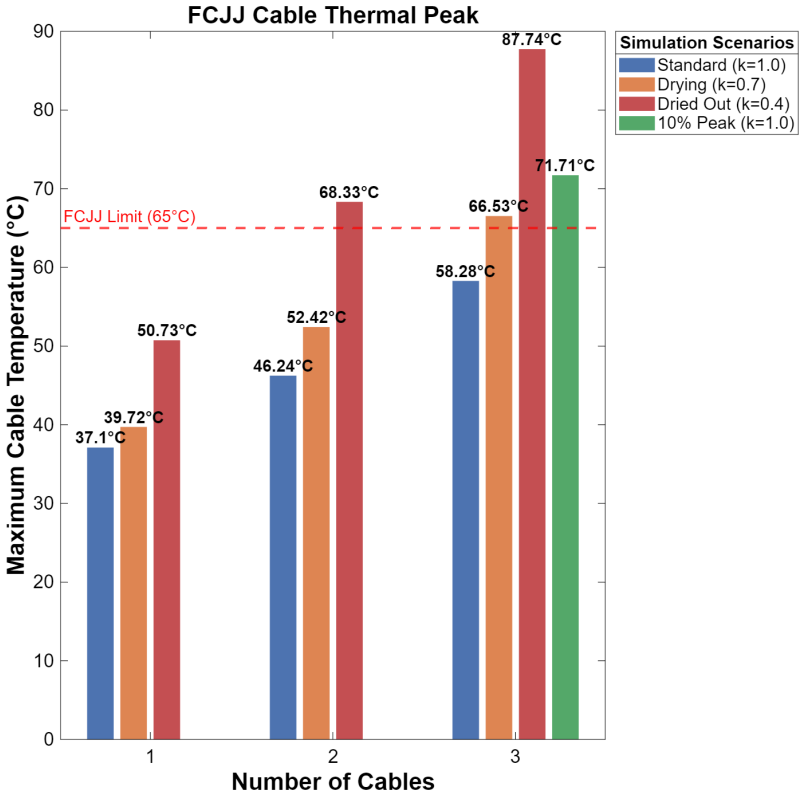

Figure 5.25: An overview of the thermal maximum of the FCJJ cable simulations.

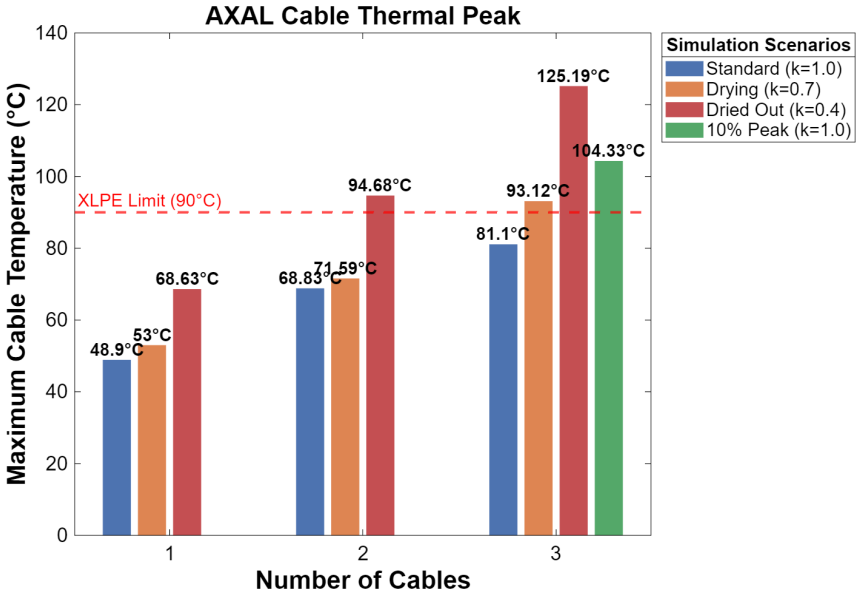

Figure 5.26: An overview of the thermal maximum of the AXAL cable simulations.

The results indicate that the setup is sensitive to the addition of more cables. A single cable reaches 37.1 ° C and 48.9 ° C respectably for FCJJ and AXAL, under normal conditions. This is far below the thermal ratings. Consequently, for the three cable configuration, the peak temperature increases to 58.3 ° C for FCJJ and 81.1 ° C for AXAL which, for both cables, is close to the thermal rating. Thus, these values are still considered reasonable operating points for the cables. However, any negative variation of the conditions will probably exceed the rating.

Increasing the current by 10% in the three cable setup resulted in a temperature increase from 58.3°C to 71.7°C, close to 23% for the FCJJ cable. 81.1°C to 104.3°C, close to 29% for the AXAL cable. This is because, according to (3.1), the heat generation is proportional to the square of the current. As a result, load management is crucial in the case where cables are placed in close proximity.

The reduction in the thermal conductivity of the surrounding soil was confirmed to be a significant risk to the cables. As a result, the reduction of k to 0.7 increased the FCJJ cable to 66.5 ° C and the AXAL cable to 93.1 ° C. However, in the extreme scenario of completely dried soil, the cable temperature increased to 87.7 °C for FCJJ and 125.2 °C for AXAL. As a result, both cables exceed the thermal rating in both scenarios; however, the latter poses a severe risk of permanently damaging the cables.

5.4.1 Thermal aging

This section expands the thermal aging model to quantify the impact of thermal stress for FCJJ and AXAL cables.

The aging follows the temperature and similarly the addition of more cable installations, which will directly increase the aging. Under normal conditions, the three

cables setup is below the thermal rating for both FCJJ and AXAL. However, as shown in figures 5.25 and 5.26, mutual heating has the overall greatest impact on temperature.

Increasing the current by 10%, shown in section 5.4 leads to a spike in the aging factor. The FCJJ cable, the aging factor increases from 0.47 to 2.1 and thermal aging increases from 47.5 to almost 147 days. With the AXAL cable, the aging factor increases from 0.37 to 4.8 and the total aging increases from 7.7 to 59.5 days. As a result, higher current peaks during a cold winter period can severely degrade cables.

Similarly, with the results of Section 5.4, shows that the drying of the soil results in an increase in temperature. The scenario in which the soil is dried could lead to catastrophic damage. As a result, FCJJ faced an equivalent aging of 517 days with a maximum aging factor 10.8. The AXAL aged 380 days and reached a factor of 37.8 at the same time.

As shown in the figures in section 5.3 and calculations with Arrhenius equations, the AXAL cable has a higher exponential spike increase in the equivalent aging during the temperature rise above the rated temperature. Although FCJJ had a linear increase with aging, overall it ages more except in the last scenario.

6
Discussion

As stated in chapters 2 and 3, the cable temperature gets influenced by numerous factors, like soil temperature, load current and placement of the cables. There are two distinct approaches to calculating the temperature of the cable in COMSOL. This section will discuss the use of COMSOL, the environmental impacts, mutual heating, aging and limitations.

6.1 Model complexity

The decision stated to utilize a 2.5D model in section 4.4 was influenced by the need for both accuracy and computational time. However, a 3D simulation will be more complex and have a result with higher accuracy for the temperatures and magnetic fields. The 2.5D model with a symmetry of 1 meter of depth, collectively, computes effectivity enough data required for a sensitivity analysis.

Additionally, in section 5.2 the AXAL induction heating and the heat source models temperature profile showed very similar results with approximately identical pattern. This validates the use of the simplified heating model for models with higher design complexity. This reduces the simulation time while maintaining high accuracy. Using this methodology when designing for larger cables with higher voltages, consider the skin effect. In Section 3.4 the skin effect starts to have a larger impact on the cable losses, making it impossible to neglect. Therefore, in those scenarios, the model will need to use the induction heating with stranded conductors.

Lastly, as stated in section 4.9 the FCJJ cable has less complexity in its design. Induction heating is thus preferable, since the model already computes the result relatively fast. That means that no compromise is needed. Thus, the model can additionally compute the magnetic field data, which is beneficial.

6.2 Weather and environmental impact

With the results observed in section 5 the peak load occurs during winter, typically due to the increased electricity demand at that period. However, the risk during summer cloud theoretically pose a risk for the extended lifespan of cables. Higher temperatures during warmer periods could dry out the soil in addition, which would further decrease the thermal conductivity. Increasing the strain on the grid due to the continuous growth of the electrification increases the risk of higher peaks. As shown in section 5.4, the 10% current increase has an impact on the temperature profile. Possibly, if the peak is even bigger during a drying period in the summer, it will be closer to or above the rated temperature.

In the soil drying scenario explored in section 5, both AXAL and FCJJ with three cables exceeded the thermal rating, and for the dried soil, it exceeded the rating by a wide margin. Within that period, the AXAL cable reached a maximum temperature of 125.2 ° C, as shown in figure 5.14d. This period creates thermal instability. When the soil dries, its heat dissipation decreases, increasing the temperature and dries the soil even further.

6.3 Mutual heating

Defining in section 2.4.2, the addition of cables will increase the temperature. A finding with the results is the large impact of the mutual heating when a new cable is placed in close proximity. In addition, with the single and double cable configuration, both the FCJJ and AXAL cable were below the rated temperature, for both scenarios, with margin to spare.

Despite this, the addition of the third cable adds more complexity. The soil temperature increases in general with the additional heat source, reducing the gradient between the cable temperature and its surroundings. As a result, the cables operate on a narrow margin, where the system is sensitive to external factors. Although cable placement is set in existing installations, exploring the width of the space between cables is an alternative. The cost of installation is high, and increasing the space for the cables would drive it up further. However, as mentioned in section 2.4.2, a higher gap would decrease mutual heating and the collective temperature of the cable. Thus, gives the possibility of lowering the aggregate cost since the cables will have a longer lifetime.

6.4 Arrhenius aging

The main source of cable aging is thermal stress on the insulation material. The Arrhenius equation describes the effect of temperatures on aging. The implementation of the Arrhenius equation, summarized in Sections 5.3.1 and 5.4.1, highlighted that thermal aging is not linear, which results in an exponential increase in the aging factor when operating above the rated temperature. The scenario with the 10%

increase in current for three XLPE cables. Defining in 5.8, the thermal aging factor at its peak increased to 4.8 times higher than designed for.

Furthermore, it is apparent that when operating below the rated temperature, the thermal lifespan of cables can be longer than its expected lifespan. Thus, XLPE operating in 70°C ages at a tenth of the speed.
The older FCJJ cable did exhibit a distinct linear profile, while also operated closer to the thermal rating. Thus, potentially making it more vulnerable to slight changes in load. Explained in section 4.11, XLPE uses a higher activation energy which, with the thermal aging results, demonstrates that the activation energy affects the outcome more when the temperature increases.

6.5 Result limitations

Although the results presented in this thesis are theoretically and physically grounded, some results for extreme scenarios should be interpreted with a degree of caution.

COMSOL has preset values for different materials, however, most designs rely on specific material and geometric assumptions to simplify the potential complexity of real life models. Precise material parameters and geometric measurements for cables are difficult to source, as manufacturers do not publish data publicly. Thus, with assumptions being a requirement, it may introduce deviations from real performance.

Additionally, the FCJJ cable is an older model that is still in operation in certain areas. A cable model that has been operating over decades may have deteriorated, with the possibility that the actual properties and parameters of the cable have decreased. Therefore, the real life cable could have worse thermal characteristics, conductivity and dielectric than the idealized parameters that were assumed for the simulation.

In these simulations, soil drying was applied to the entire surrounding area and throughout the day. For observing the different seasons throughout the year. Realistically, soil often dries in hot spots confined to the proximity of conductors. Choosing this simulation route may lead to different thermal behaviors. Furthermore, the completely dried scenario of 0.4 [W/(m· K)] mentioned and used in section for the simulations probably will not occur but should be seen as a worst case scenario.

Lastly, it is important to mention that an electrical grid employs relay protection and monitoring systems, mentioned in Section 3.6. In actual scenarios, it would be extremely likely that the system intervenes if the current or temperature reaches these high values. In particular, these extended periods of time above the thermal limit are unlikely to occur.

6.6 Sustainable and ethical aspects

The primary incentive for optimizing current capacity for underground power cables is to meet the increasing electricity demand driven by the electrification of society. Improving and understanding existing grid is essential for increasing its efficiency, in addition to when installing new cable lines. Thus, Understanding thermal aging and the parameters affecting it, with mutual heating, soil thermal conductivity and the load can help operating more safely and increase its lifespan. With dynamic cable rating its possible to operate near the thermal limits without risking breakdown. These preventive measures will reduce the risk of new installations, which will safe much on raw materials for the new cables. In addition, save on green house emissions that is associated with new infrastructure projects. Consequently, maximizing the lifespan of the cable will increase its sustainability.

From an ethical perspective, the consequences of being close to the rated temperature are more nuanced. Particularly the older FCJJ model, that carries a higher risk when exposed to temperatures over the thermal limit. Reaching above the rated temperature can lead to breakdown or failure. This will result in power outages that often affect vulnerable individuals or crucial infrastructure more. In addition, these breakdowns can lead to the pollution of surrounding environment with the leakage of non environmental friendly materials.

Last, relying on dynamic cable rating and monitoring systems of the grid will increase the knowledge of its vulnerability. By ensuring that breakdowns can be monitored and prevented with the help of authorities and that its handled with the responsibility it needs. Thus, the sustainable benefits of optimizing the cables thermal limit with monitor systems seems to outweigh the disadvantages ethically.

7
Conclusions and Future Work

7.1 Conclusions

The result of this thesis establishes a modeling framework to analyze the thermal aging of underground cables for 10 kV with varying stress on the load, by soil droughts or current spikes. By integrating the COMSOL temperature results with the Arrhenius equation, the study quantifies the insulation lifespan impact of current spikes, mutual heating, and the soil's thermal conductivity.

Additionally, this thesis concludes that the one or two cable configurations are thermally stable at these gaps between the cables. If a new cable line was needed and only one to two cables were needed. The new installation will handle loads higher than currently operating and also unexpected environmental fluctuations. Despite this, the three-wire configuration is at greater risk and operates with thinner margins under normal conditions. The thesis has identified a thermal threshold with the three cable setup. The temperate of the soil increases substantially, which reduces the ability of the surrounding soil to dissipate heat. However, if the placement of the cables can be further away, the temperature would decrease.

Furthermore, the sensitivity analysis validated that the thermal conductivity of the soil can possibly drive thermal aging more than the load peaks. In the most extreme scenario, the AXAL cable reached a maximum aging factor of 37.8. This implies that a day of operation at these temperatures results in almost 38 days of aging of the insulation. When comparing the different peaks of the aging factor with the thermal peak, a can draw the conclusion that the aging factor increases exponentially. A similar result for the FCJJ cable, reaching a maximum aging factor of 10.8. However, these are not realistic scenarios overall due to the grid's protection systems that would mitigate the current and temperature. Additionally, the soils lowest conductivity of 0.4 [W/(m· K)] is an extreme scenario with a low probability of happening. Understanding the potential damage that could be caused by excessive temperatures is crucial for cable design. Additionally, shown with values closer to normal conditions, the surrounding soil moisture will affect the thermal conductivity, which can dry out and fluctuate over time.

Lastly, examining the three cable configuration in general, the setup can potentially have an increased load if desired or accidentally during the late spring, summer, and early and autumn periods for both cables. Even if the margins are thin during

normal winter conditions, operating over rated temperature during a short period of time with a new AXAL cable, the damage is unlikely to be significant. Observing the current peak simulation, the overall aging was well below a year for both cables. However, the FCJJ cable, with the older age, additional concerns may arise if exposed to higher temperatures and is not recommended.

7.2 Future work

To build on the simulation of this thesis, a few topics need to be broadened and further researched. However, the thesis used a 2.5D simulation design to have efficient and accurate simulations. Future research should explore a 3D layout to investigate regional hot spots. It could also be interesting to explore the impact of cable joints, where faults often occur. Additionally, different phenomena and placements can be simulated that impact heating and aging. Examples could be PD-discharges, corona discharge, and design of cables laid in tunnels. These can be investigated to expand the scope and understand the impacts of thermal aging of cables.

The data for the cables were difficult to collect, which required assumptions to complete the design. If possible, source data for the material properties from the manufacturer for higher accuracy would be recommended. In addition, since the FCJJ cable has been in service for decades, more accurate activation energy and other parameter values should be considered. Taking into account the already degrading values and alternatively testing the properties of the aged oil impregnated paper. In addition, for the soil, more accurate data could give more accurate results. Future models could benefit from measured data from soil temperature, not assumptions derived from air weather. The soil's drying model needs modification, allowing a step function to change the conductivity over time or to model moisture migration. This would make it easier to identify the temperature at which soil moisture begins to move away. The latter would be the most accurate, but adding a considerable amount of complexity to the model.

The implementation of the mesh is crucial for accurate and fast simulations. Investigating an implementation of a local finer mesh in the complex part of the design, with the rest having a coarser mesh is needed. Potentially, resulting in a similar result with a shorter simulation time.

Investigating cable placement could be a priority. The mutual heating had a large impact on the overall temperature. One way of mitigating the temperature is to move the cables farther away. Even if placing the cables with more space in between is possible, perhaps there are other factors that would not allow it. Strict building regulations or costs could stop projects with a larger space between. However, the situation should be explored to understand better the effects of mutual heating on underground cables. Lastly, the load at periods of lower demand is expected to increase in the coming years. With peaks from electric vehicle charging, AI uses and solar panels operating during summer, leading to higher loads with less downtime. Exploring future scenarios with assumptions for the load at these times

is recommended to analyze the increased impact of aging.

Bibliography

[1] Göteborg Energi Nät AB, "Nätutvecklingsplan 2025 - 2034," Rep. 20-2024-0318, May 2024.

[2] A. Sturchio, G. Fioriti, M. Pompili och B. Cauzillo, ”Failure rates reduction in SmartGrid MV underground distribution cables: Influence of temperature,” AEIT Annual Conference-From Research to Industry: The Need for a More Effective, 2015.

[3] M. Taljegård, T. Lundblad, Y. Kobayashi, E. Nyholm, and P. Blomqvist, "Påverkan på elsystemet och elnätet av en storskalig elektrifiering av fordonsflottan: Ett elsystem för elfordon," Energiforsk, Stockholm, Sweden, Rep. 2023:966

[4] J. D. Jackson, Classical Electrodynamics, 3rd ed. New York, NY: Wiley, 1999, pp. 184–198.

[5] F. P. Incropera, D. P. DeWitt, T. L. Bergman, and A. S. Lavine, Fundamentals of Heat and Mass Transfer, 7th ed. Hoboken, NJ, USA: Wiley, 2011.

[6] P. Cygan och J. R. Laghari, ”Models for insulation aging under electrical and thermal multistress.,” IEEE, vol. IEEE Transactions on Electrical Insulation, nr 25.5, pp. 923-934, 1990.

[7] G. C. Montanari och G. Pattini, ”Thermal Endurance Evaluation of Insulating Materials: A Theoretical and Experimental Analysis,” IEEE Transactions on Electrical Insulation, Vol. %1 av %2vol. EI-21, nr no. 1, pp. 69-77, Feb. 1986.

[8] M. MöllerJensen, ”Overload Capacity of Polymer Insulated Medium Voltage Cables,” DTU, 2011.

[9] NKT Cables, ”Kraftkabelhandboken från NKT cables”

[10] Svensk Standard, SS, ”424 14 24„” Kraftkablar–Dimensionering av kablar med märkspänning högst 0, 6/1 kV med hänsyn till belastningsförmåga, skydd motöverlast och skydd vid kortslutning, nr 6, 2005.

[11] K. Malmedal, C. Bates och D. Cain, ”The Heatand Buried Cable Conundrum: A Method to Help Determine Underground Cable Ampacity,” IEEE Industry Applications Magazine, vol. 22, nr 5, pp. 20–31, 2016.

[12] International Electrotechnical Commision (IEC), ”Electric cables - Calculation of the current rating. Part 3-1: Sections on operating conditions - Reference operating conditions and selection of cable type,” 1999.

[13] G. J. Anders, Rating of electric power cables: ampacity computations for transmission, distribution, and industrial applications, New York: Institute of Electrical and Electronics Engineers, 1997

[14] R. Bartnikas och K. D. Srivastava, Power and communication cables, McGraw-Hill, 2000

[15] Nexans, ”60-500 kV High Voltage Underground Power Cables - XLPE insulated cables”.
[16] D. Karlsson, F. J. Sollerkvist och J. Lundquist, ”A comparison of XLPE cables and overhead lines,” STRI, 2001.
[17] D. W. Pryer och P. F. Gale, Electrical Engineer’s Reference Book (Fifteenth Edition). Pages: 23/1 - 23/43, Oxford: Newnes, 1993.
[18] EPRI, ”Increased Power Flow Guidebook - Underground Cables,” EPRI, Palo Alto, CA, 2003.
[19] M. H. Shwehdi, M. A. Morsy och A. Abugurain, ”Thermal aging tests on XLPE and PVC cable insulation materials of Saudi Arabia,” i Electrical Insulation and Dielectric Phenomena. Annual Report. Conference on (pp. 176 180). IEEE. , 2003
[20] I. Mladenovic and C. Weindl, "Empiric Approach for Criteria Determination of Remaining Lifetime Estimation of MV PILC Cables," in Dielectric Material, M. A. Silaghi, Ed. Rijeka, Croatia: IntechOpen, 2012, ch. 11, pp. 251–276. doi: 10.5772/51490.
[21] Recommendations for additional testing of submarine cables, CIGRÉ Technical Brochure 722, Working Group B1.52, Paris, France, Aug. 2018.
[22] Recommendations for testing of Long HVDC Extruded Cable Systems for Power Transmission at a Rated Voltage up to 800 kV, CIGRÉ Technical Brochure 496, Working Group B1.32, Paris, France, 2012.
[23] International Electrotechnical Commision (IEC), ”IEC 60853-2. Calculation of the cyclic and emergency current rating of cables. Part 2: Cyclic rating of cables greater than 18/30(36) kV and emergency ratings for cables of all voltages,” IEC, Geneva, Switzerland, 1989.
[24] S. T. Larsen, C. L. Ong-Hall och P. L. Stephenson, ”Cable rating methods applied to a real-time cable system monitor,” i Power Cables and Accessories 10kV-500kV, 1993., Third International Conference on, 1993.
[25] nkt cables, High Voltage Cable Systems: Cables and Accessories up to 550 kV, Cologne, Germany: nkt cables, Mar. 2009. [Online]. Available: www.nktcables.com
[26] U. Khan et al., "Continuous Markov-Based Reliability Analysis of Underground Distribution Power Systems Under Temperature and Load-Dependent Failures," IEEE Access, vol. 13, pp. 207651-207664, Dec. 2025.
[27] IEEE Standard Power Cable Ampacity Tables, IEEE Std 835-1994 (R2012), 1994.
[28] NKT, "AXAL-TT PRO 3.0 Endurance 12/20 (24) kV: Medium Voltage Cables with XLPE Insulation," Technical Data Sheet, May 2023.
[29] Göteborg Energi Nät AB , Schaktsektioner , Drawing No. 3001 , Oct. 7, 2021.
[30] IEC 60287-3-1: Operating Conditions - Site Reference Conditions.
[31] COMSOL, "Submarine Cable 6 Thermal Effects," COMSOL Multiphysics Application Library, `ACDC_Module/Tutorials,_Cables/submarine_cable_06_thermal_effects`, ver. 6.3.
[32] Sveriges meteorologiska och hydrologiska institut (SMHI), "Ladda ner väderobservationer – Lufttemperatur (Station 71420: Göteborg A)," SMHI.se. [On-

line]. Available: https://www.smhi.se/data/hitta-data-for-en-plats/ladda-ner-vaderobservationer/airtemperatureInstant/71420.

[33] O. Boyarkin and R. H. W. Hoppe, "Optimal control of inductive heating of ferromagnetic materials," Russian Journal of Numerical Analysis and Mathematical Modelling, vol. 28, pp. 101–123, 2013. https://doi.org/10.1515/rnam-2013-0030

[34] A. M. Emsley and G. C. Stevens, "Kinetics and mechanisms of the low-temperature degradation of cellulose," Cellulose, vol. 1, pp. 26–56, 1994.

[35] J.-P. Crine, "A Molecular Approach to the Electrical Aging of XLPE Cables," i Jicable, 2007.

DEPARTMENT OF ELECTRICAL ENGINEERING
CHALMERS UNIVERSITY OF TECHNOLOGY
Gothenburg, Sweden
www.chalmers.se

CHALMERS
UNIVERSITY OF TECHNOLOGY